Neural Targets of Electric Field Stimulation

by

Thomas Radman

A dissertation submitted to the Graduate Faculty in Biology in partial fulfillment of the requirements for the Degree of Doctor of Philosophy, The City University of New York

2009

This manuscript has been read and accepted for the
Graduate Faculty in Biology in satisfaction of the
dissertation requirement for the degree of Doctor of Philosophy.

Thomas Radman

Date — Chair of Examining Committee

Marom Bikson

Date — Executive Officer

Lucas C. Parra

Christopher Y. Chan

Joshua C. Brumberg

Raddy L. Ramos

Supervisory Committee

THE CITY UNIVERSITY OF NEW YORK

Abstract

NEURAL TARGETS OF ELECTRIC FIELD STIMULATION

by

Thomas Radman

Advisor: Professor Marom Bikson

Clinical application of electric fields to the brain are promising non-invasive approaches for the treatment of psychiatric, neurological, and pain disorders. Low-magnitude electric fields, which do not cause neuronal firing but only create changes to the voltage necessary for inducing neuronal firing by approximately 1%, are known to have substantial behavioral effects and therapeutic outcomes. Transcranial direct current stimulation is one electric stimulation modality that induces such low-magnitude electric fields. Electric fields of magnitude sufficient to directly trigger neuronal firing may be induced by transcranial electric stimulation and transcranial magnetic stimulation. Many therapeutic advances have been made using these techniques, and they create new experimental approaches to increase our knowledge of how the brain works. Still, the fundamental mechanisms as to how these electric fields may affect neuronal elements of the brain are not fully understood. Chapter 1 of this thesis creates a mechanistic model describing how an electric field of any small magnitude may still have an effect on neuronal processing by changes in spike timing. This mechanistic framework has implications for the effects of endogenous, brain-generated electric fields as well as electric stimulation modalities. The second chapter of this thesis develops a model of how cortical neuronal morphology and cell type may be used to predict changes in polarization and firing caused by electric fields. Both of these studies employed techniques to record from single cells in the brain, and all models described have been experimentally verified through these techniques.

Preface for my Family and Friends

Mrs. K, a recent case study of depression reported by the University of Pennsylvania Comprehensive Depression Center, had run out of options. Antidepressants and psychotherapy had failed her, and she was in the throes of her third major depressive episode. Assessing the options available for treatment-resistant patients, she made the decision to try transcranial magnetic stimulation (TMS), a therapy that places an electromagnet next to the scalp that interacts with the ongoing electrical activity of the brain in a focal, non-invasive manner. At the time, TMS was not approved by the FDA for the treatment depression but TMS was the correct treatment for Mrs. K and her depressive symptoms went into remission.

Transcranial magnetic stimulation was approved in October by the FDA for the treatment of depression, and the decision Mrs. K faced has been made easier for both patients and the prescribing. Further research, with larger study groups, are needed to confirm the efficacy of TMS as compared to other therapeutic options. FDA approval is a promising step towards making TMS a viable treatment alternative for patients not responding to other approaches. With TMS, an electromagnet creates a magnetic field that is unimpeded by the skull. This allows the induction of focal currents in the brain, causing neurons to fire action potentials, potentially leading to short and long-term therapeutic changes. As with any therapy, not everyone responds to TMS, and the challenge facing researchers is making the changes last longer through maintenance TMS sessions. The treatment is generally painless with no side effects, with the exception of occasional headaches that subside within hours after

the treatment (the discharging electromagnetic creates a clicking sound, can slightly activate muscles near the magnet, and light vibrations can be felt on the skull).

To date, the only proven non-invasive treatments for depression are psychotherapy, pharmaceutical anti-depressants and ECT. ECT is considered the most effective anti-depressant intervention as statistically the highest percentage of patients respond to it, but the treatment induces seizures and is associated with side effects like temporary memory loss. It also has a reputation as a disturbing treatment reserved for only the most extreme cases of depression. In the 1975 film adaptation of One Flew Over The Cuckoo's Nest, R.T. McMurphy, played by Jack Nicholson, is forcibly given ECT by cruel and distrustful doctors. Conversely, TMS has little cultural stigma. It was portrayed in a 2007 episode of the medical TV drama House as a casual treatment applied to a teenage patient during a casual conversation. TMS provides patients with hope of the response rate of electro-convulsive therapy (ECT), without the side effects or stigma.

While pharmaceutical approaches are preferred by many doctors, many patients do not respond to drugs, and if they do, the response can take up to four weeks. TMS can create an immediate effect in the brain, such as triggering a muscle twitch when the motor cortex is stimulated, or the induction of phosphenes during stimulation of visual cortex. This immediate impact is being investigated to expedite TMS as a therapy, which is currently considered to take a few weeks of repeated treatments. Patients also experience side effects such as weight gain, fatigue, and insomnia due to diffuse distribution of the drug in the blood stream, which leads to discontinuation of use for some patients, the stigma of taking pills daily, and potential liver damage that for some can outweigh any gains achieved.

Depression occurs when the communication between brain cells gets interrupted, causing the connection between the cells to weaken. The pruning of inefficient connections is a natural part of how the brain maintains its efficiency. During youth we haveour greatest number of unspecified brain cells, and throughout our lives we strengthen the connections we regularly use and weaken or remove the connections we don't use. This is part of the reason why it is easiest to learn a foreign language or musical instrument when we are younger. In depression, a malfunction in the production of neurotransmitters used for neural communication leads to over-pruning of connections used to control mood. This is where TMS and pharmaceutical approaches share the approach of targeting these weak neural connections. Pharmaceutical anti-depressants manipulate the neurotransmitters that pass neural codes (action potentials) between brain cells, improving the efficiency of neural communication. TMS causes the cells passing neural codes to fire together in response to the magnetically-induced currents, and this coherent communication is thought to lead to a strengthening of the connections that have been weakened by depression.

In addition to FDA approval as a treatment for depression, TMS is also approved for peripheral nerve stimulation to treat movement disorders and has been used for other disease treatments in an "off-label" manner, which means a non-FDA approved prescription of a drug that has been approved for the treatment of another illness. For example, a doctor may prescribe anti-epileptic medications to patients with bipolar disease, even though it has not formally gone through the FDA approval process for that application. Electrical stimulation of the brain in the form of implanted electrodes has also been successful for treatment of Parkinson's disease, Epilepsy, and Depression. Some extremely low-power electrical

stimulators are already FDA-approved for purchase through your doctor, and simple enough to be used at home for alleviating some of the symptoms of depression. In Europe, where regulations are different than those of the FDA, some patients have been given these stimulators to bring home to treat migraine. Implanted electrodes in the spinal cord are approved to treat pain. The most well-known electrical intervention for the body is the cardiac pacemaker.

TMS is not 100% effective as a treatment for depression, and it has been cleared for use only in patients who have not responded to at least one antidepressant medication. The evidence for TMS application in depression shows great promise, as researchers diligently work to unravel the mechanisms behind how it can most effectively modulate nervous system function. Its approval by the FDA speaks to its safety, and will encourage more doctors to try it as another approach for treatment-resistant patients. The rate of production of new drugs to treat mental illness has decreased over the last ten years, many of them so-called "me-too" drugs that are just small isomeric changes to already existing anti-depressants. New laws concerning patent protection duration and an influx of generic drug versions has decreased the monetary gain of research and development for pharmaceutical companies.

It remains to be seen if TMS will blossom into a viable alternative for the depressed population. Larger study groups observed for a longer period of time is necessary, and the recent fda approval is an important milestone towards achieving this. Clinical studies are continuing, and President Barack Obama has pledged stimulus money to the NIH, some of which will go to TMS research. The pharmaceutical industry grew exponentially and is now

suffering a turbulent fate. It remains to be seen if the non-invasive therapeutic medical device industry can experience growth without similar fallout.

My thesis has investigates the effect of the electric fields induced by these non-invasive electrical therapies at the resolution of a single cell in the brain. I have employed the techniques of the cellular electrophysiologist to *in vitro* (dissected outside of the living organism) brain circuitry models. Countless advances to the understanding and use of pharmaceutical drugs as therapy have been accomplished through similar techniques. It is the hope of the basic researchers of electric field stimulation, that countless advances to the understanding of non-invasive electrical therapies shall occur through our efforts. In the meantime, a new hope for the treatment of depression looms on the horizon, and hope has always been the best treatment for depression available.

Acknowledgments

First of all, thanks to Madeline for whom this accomplishment is equally hers. Enough cannot be said for her support, understanding, and love. To Madeline again, for her help in writing the Preface. Thanks to Mom for giving me every chance to obtain a PhD. Micheal, Terri, Jen, Matt, Ben, and Grace for support, and patience in listening to stories about research. Sincere thanks to my thesis committee for their advice and guidance. To Marom for balancing patience for my mistakes, while giving me independence to find my own way. Lucas never fails to impress with his mastery of his field. Chris for some of the most intellectual conversations I've had. Josh for accepting me like a student from his own lab, and for his generosity with his time. Raddy for defining to me what it means to be a young scientist.

Individual thanks during the course of the thesis research go to: Abhishek Datta, Reem Khalil, and Jonathan B. Levitt of the City College of New York; Chris Leonard of New York Medical College; Denis Paré of Rutgers University; Jack Belgum, Adair Oesterle, and Rick Ayer of Sutter Instruments; Tim Bergel and Simon Gray of Cambridge Electronic Design (CED); Zhi-De Deng, Angel V. Peterchev, Sébastien J. Thuault and Stephen A. Siegelbaum of Columbia University, Boris Heifets and Pablo Castillo of Albert Einstein College of Medicine of Yeshiva University; Natascia Vedovato and David C. Gadsby of Rockefeller University; Jimmy K. Duong of the Irving Institute Biostatistics Consultation Service.

Table of Contents

List of Figures

List of Tables

Chapter 1

Introduction

1.1.0 An experimentalist approach to clinical brain stimulation

Basic science research has been instrumental to the advances of pharmaceutical therapies for mental illness and pain disorders. Non-invasive electric field based therapies have recently been FDA approved for the therapy of treatment resistant depression (specifically TMS, transcranial magnetic stimulation), and the number and size of established clinical research labs has experienced tremendous growth in the past decade (most prominently for the techniques of TMS and tDCS, transcranial direct current stimulation). Despite the contributions of basic science to pharmaceutical therapies and the obvious potential of electric field based therapies, there are just a small number of basic research laboratories working to understand the mechanisms of these electric fields, using the tools of cellular electrophysiology. This understanding begins at the level of a single cell of the mammalian brain network. With greater than 90% genetic similarity to humans, we have employed the methodology of rat brain slice preparation and incubation. The tools used in this thesis are sharp electrode somatic recordings, and whole-cell patch clamp somatic recordings. For these respective techniques, the rat age, slice preparation techniques, and recording equipment must be selected to optimize the probability of the researcher to make an electrical connection with the neuron, and to prolong the recordings for sufficient duration to complete the necessary experimental paradigm in order to investigate the hypothesis in question. These techniques should be viewed as a necessary complement to extracellular, and *in vivo* recording methods as any of these methods in isolation lead to a skewed view of neuronal activity but in combination they may be used to rationally understand the response of the brain to a natural or electrical stimulus input to the neuronal system.

1.1.1 Unanswered questions: Can long term plasticity be extended as a suitable clinical therapy?

Despite the growing rate of clinical research in the field of non-invasive electric field-based therapies, there is still uncertainty on it's applicability for mental illness intervention and maintenance. The main issue limiting the use of electric fields as therapy is the duration of the plastic changes induced in the brain. Though FDA approved for treatment resistant depression, TMS requires specifically scheduled maintenance pulses to be re-applied. Many patients do not respond to the therapy at all, or go into remission during the course of treatment. tDCS has only been used in a few controlled clinical trials as a therapy for depression.

TMS test pulses to motor cortex resulting in motor-evoked potential (MEP) responses are commonly used to test the duration of plastic brain changes induced by repetitive TMS (rTMS) pulse trains, or anodal or cathodal tDCS induced plastic brain changes. The MEP is the response of descending corticospinal tract outputs at the targeted muscle, commonly FDI (first dorsal interossesous) or EDC (extensor digitorum communis); small muscles on the digits of the hand. These are slower compound muscle action potentials (cMAPs) that may be observed when recording epidurally at the spinal cord as the summation of direct and indirect waves (d-wave and i1, i2, i3 waves, of successively longer latencies). In response to a TMS pulse to motor cortex, d-waves are typically only thought to be elicited by lateral-medial (L-M) oriented coils, using higher intensities of stimulator output, possibly due to the depth of the layer 5 corticospinal output cells. The most common clinical paradigms employ anterior-posterior (A-P) coils, and thus are thought to indirectly activate the corticospinal tract, and only directly activate afferent input to the targeted cortical area. Behavioral reports (e.g. phosphene threshold) and changes (performance on psychophysical tests) may also be used to assess plasticity changes.

Long-term depression (LTD) may be induced by low (~ 1 hz) frequency rTMS or cathodal tDCS, while long-term potentiation (LTP) may be induced by higher frequency and theta burst rTMS as well as anodal tDCS and recently transcranial random noise stimulation. Typically these plastic changes do not persist on the scale of hours and at most one day.

LTP in the hippocampus occurs when afferent input excites a threshold number of excitatory synapses (Sayer et al. 1990, Malinow 1991), and when postysynaptic dendrites in the region of active synapses are sufficiently depolarized to permit Ca2+ entry. In cortex, weak steady currents potentiate somatosensory cortical response (Bindman et al., 1964). The highest probability of LTP rate is in rat age 21 to 34 days. Experiments showed that postsynaptic LTP was only induced by an EPSP when paired with current injection, but was less frequent in vitro than in vivo maybe because of lack of modulatory inputs (Bindman and Murphy, 1990). In other experiments, homosynaptic LTD was dependent on the level of depolarization and was postsynaptic (Artola et al., 1990).

In addition to the induction of plasticity, TMS is also used experimentally to jam a brain area during a behavioral task ("online" TMS), and thus the causality of that area to a behavioral task may be assessed. Research is ongoing to use the response to single test pulse (TMS-evoked response) as a measure of normal or abnormal brain function.

1.2.0 General Methods

In the ever-changing field of cellular electrophysiology, the best resource to learn about the latest techniques is to talk to the experts. Throughout my efforts to achieve proficiency in these challenging techniques I have contacted and have been welcomed by some of the best

known scientists in their field. I have always tried to properly acknowledge those who have contributed to an individual chapter in the appropriate section, and these people should be commended for their excellence as well as their willingness to share. This extends beyond the realm of academia, to the support personnel of the manufacturers of the respective equipments used, who must be considered as a resource to further an investigators knowledge of their craft.

1.2.1 Brain Slice Prepration and Incubation

Hippocampal brain dissection (Chapter 1) was accomplished using the technique of cervical dislocation. Cortical brain dissection (Chapter 2)) was accomplished through the technique of decapitation. The latter technique is much easier with smaller animals, and this method allows the decapitated skull and brain to immediately drop into cooled/slushy artificial cerebrospinal fluid (ACSF) in a deep petri dish. The theory behind this is that the sooner the brain begins cooling, the less excitotoxicity will occur due to the dissection and slice preparation procedure. The brain may then be fully dissected in the cooled ACSF, and the petri dish with brain tissue therein may be rinsed through with fresh cool ACSF. All ACSF should be attempted to be bubbled for a short time before interfacing with brain tissue. The blocking procedure to be used may also be performed in the cool ACSF before placing the blocks onto the glue for vibratome cutting.

All animals were anaesthetized with intraperitoneal ketamine (7.4 mg kg-1) and xylazine (0.7 mg kg-1). Brain slices were prepared from Sprague-Dawley rats on a vibratome (Integraslice 7550 PSDS, Campden Instruments, Lafeyette, Indiana, USA) as previously described (Brumberg et al., 2000; Bikson et al., 2004; Radman et al., 2007; Ramos et al., 2008a).

The brain slices were stored in a holding chamber submerged in artificial cerebrospinal fluid (ACSF) consisting of (mM): 125 NaCl, 26 $NaHCO_3$, 3 KCl, 1.6 $CaCl_2$, 1.5 $MgS0_4$, 1.25 NaH_2PO_4, and 10 glucose, bubbled with a mixture of 95% O_2–5% CO_2 aerated with 95% O_2-5% CO_2 to a final pH of 7.4. The slices were stored in a holding chamber submerged in ACSF and bubbled with a mixture of 95% O_2–5% CO_2 at room temperature. After >60 min, slices were transferred to a submerged patch-clamp recording chamber maintained at 36°C.

1.2.2 Uniform Electric Field Generation

Uniform electric fields were generated across individual slices by passing current between two parallel Ag/AgCl electrodes (Gluckman et al., 1996; Ghai et al., 2000; Gluckman et al., 2001; Francis et al., 2003; Bikson et al., 2004; Deans et al., 2007; Radman et al., 2007) placed on the bottom of a customized chamber. The electric field (mV/mm or $mV \cdot mm^{-1}$) in the chamber was measured by two recording electrodes separated by 1 mm and calibrated to the current passed through the Ag–AgCl electrodes (Ghai et al., 2000; Durand and Bikson, 2001; Bikson et al., 2004). The voltage recorded by a field electrode (placed within 50 μm of the recorded neuron) was subtracted from the intracellular potential to obtain the transmembrane voltage and used to compensate for the exogenous electrical artifact.

1.2.3 Single Cell Electrophysiology

Electrophysiological signals were amplified (Axoclamp-2B, Molecular Devices, Sunnyvale, CA, USA) and filtered at 10 kHz (FLA-01, Cygnus Technologies, Delaware Water Gap, PA, USA), then digitized (Power 1401 ADC/DAC, Cambridge Electronic Design,

Cambridge, UK). Off-line analysis of action potential and passive membrane properties were performed using Signal 3 (Cambridge Electronic Design, Cambridge, UK).

Sharp Electrode techniques were used for chapter 1, sufficient for the densely packed somatic layer of CA1 in the hippocampus. Infrared-differential contrast microscopy guided whole cell patch clamp was employed in the less dense cortex (Chapter 2), and this also had the added advantage of allowing us to choose the specific cell types we should record.

The main trade-off with the techniques are as follows. With sharps you can use an interface chamber which has lower fluid levels and thus you need less current to generate supra-threshold fields. For LTP experiments, a major obstacle is overcoming the dechloridization of the field-generating electrodes. This typically especially occurs when waveforms are not charge-balanced (0 root mean square (RMS) power, i.e. equally positive and negative). IR-DIC microscopy requires a submerged chamber because the electrode objective. This has the disadvantage of requiring greater passed current to generate the same electric field as an interface chamber. The microscope objective in the bath also creates fluid level non-uniformities that may distort the field. That is why we removed the objective after obtaining a gigaohm seal with a neuron, but prior to breaking into the cell with reverse suction to obtain the whole-cell configuration. As an aside, with blind-patch you can use an interface chamber while having the advantages of the low-impedance patch electrode (electrically connected with greater extent of the cell membrane, easier to inject biocytin dye, dialysis of the cell contents with the electrode contents allowing for further experimental range such as the use of calcium chelators). Patch clamp also allows you to more confidentally observe action potentials outside the cell when in the gigaohm seal mode, without having the added and more difficult step of going whole cell.

Sharp electrodes similarly allow juxtacellular, or next to the cell recordings of action potentials that may be more effieient than actually impaling the cell, depending on the scientific questions being asked. The main advantage of IR-DIC patch is that you can select the exact cell type based on the image, or easily find cells in non-uniform structures, as opposed to the uniformity of CA1 (for instance layer 1 of cortex). If you are just interested in interneurons for instance, that is more efficient.

Which technique is easier? I have heard of researchers who recorded 15 patched cells in a day, the most I obtained was 5 (though the experimental paradigms were very long, and removing the microscope objective upon sealing can sometimes disturb the gigaohm seals). With sharps the most I have recorded is 5 also.

I have never tried blind patch. My feeling is that the concensus is that it is tedious, but maybe not in a dense area like CA1. There is further info on blind patch in the "Axon Guide" (section 5.3.2): http://www.moleculardevices.com/pdfs/Axon_Guide.pdf. Using the Sutter manipulator (MP-285) that can be programmed using C++, the procedure could be automated (pseudo-code: increment the manipulator into the slice, check if the resistance has increased, if not increment again, at a certain depth pull out and move over to a new spot). Also see: http://www.sutter.com/contact/faqs.html .

In addition to the water-based manipulator used to obtain sharp recordings in this thesis, for some pilot experiments I've used our patch clamp manipulator to also obtain some sharp recordings on the interface chamber rig. The "steps" of the motor are set to about 5 um, so based on the idea of a 10 um cell body, you won't "jab" past a cell.

The narashige MWS-32 manipulator used here has a water based remote 4th axis

(diagonal) that sits off the floating table. The problem with water based is that the water evaporates, leading to instability, so you want to get them calibrated by Narashige reps (you can make an appointment to meet them at SFN if you bring your manipulators). The problem with Narashige is that they are metric so you need to get a special adapter plate from Narashige in order to install to the Axoclamp headstages (US measurement units) as close as possible to the manipulator. It is not recommended to use the long plastic pole that comes with and screws onto the axoclamp headstage (vibratory principles of a diving-board). These water based manipulatorss have a 2mm range on their 4th axis, but are most stable between 1 to 1.5 mm, reset a new run through the slice to 1 mm and proceed down from their. Narashige representatives report their oil-based manipulators are the most stable. The stability of the manipulator may be observed by visualizing the electrode under a microscope and quantifying the drift over the course of an hour and also ensuring little to no vibrations on your recording table.

When penetrating through the slice with the stepper motor or water-based manipulator, jab forward with a quick 5 μm turn of the 4th axis, while simultaneously buzzing on the axoclamp remote buzz box. Turn back 5 μm if no cell was found, to return to the starting spot. Then perform a double jab, 5 μm to go to the spot we know there is no cell, and then another 5 μm jab with a simultaneous buzz (into an untraversed region). Keep repeating this to saw through the slice. The art of the technique is observing the voltage fluctuations and knowing if you should pull back slowly, jab a little more forward, buzz, or go slowly forward.

It is recommended to replaced the resistor-capacitor circuit that controls the time constant of the axoclamp remote buzz box, so the scale is from 1 to 5 ms instead of 1 to 50, and thus

much more sensitive. You can increase the buzz duration gradually if you cannot penetrate a cell. Molecular Devices support should be able to assist with this modification in the future. In short, in the Remote Buzz circuit change the C1 capacitor to 0.022 μF and change the R4 resistor to 4099 ohms. This will change the range to 0.1 - 10 ms. The circuit diagram is in the axoclamp 2B manual. Buzz operates by temporarily increasing the effective setting of the cap neutralization. If the headstage has some capacitive load and the cap neutralization is not advanced then the oscillation could be weak or not at all. Turn the capacitive compensation knob on the axoclamp to make the buzzes even faster than without this knob. Turn it up until you get ringing and then turn it down half a turn. We here turn it all the way back down (carefully) after impaling a cell. You don't necessarily need to use the buzz switch on the remote box, but can sometimes impale just from the jab.

The Sutter P-97 puller typically is set to obtain resistances between 60 to 100 MΩ for sharp electrode recordings. The box filament is used because it heats evenly on all sides of the electrode. Getting up above 100 MΩ, you get too wispy a tip that just deflects on the surface of the slice and you never get a cell. A symptom of this would be getting some responses upon dropping down to the surface of the slice but turning the 4th axis does nothing. We used borosilicate glass. Aluminosilicate may be better. It is half way to quartz in mechanical properties. Quartz would be the ideal, but that would necessitate Sutter P-2000. Thick walled glass in general allows for long, sharp, strong electrode tips. It is easier to get short, fine tips with 1 mm glass than with larger glass. The settings of the puller are crucial. The Air Mode of the <Delay> functions as follows: 1) the heat comes on and melts the glass. 2) the velocity transducer picks up on the movement of the puller bars (which correlates to the viscosity of the

glass) and when the velocity is reached, this is the trip point for turning off the heat, starting the cooling (a setting of 40 milliseconds if you are in the time or delay cooling mode). But in the delay mode, the total duration of cooling is 300 milliseconds (45 milliseconds more than what is offered in the time mode) and what you are delaying is the initiation of the hard pull. So, the higher your delay, the more you delay the hard pull and the more cooling the glass receives before you give the hard pull. Therefore the glass is more viscous and will not pull out as long or as small. If you reduce the delay, the earlier you pull on the glass so it is pulled at a point when the glass is not cooled as long and here the taper will be longer and the tip smaller since the pull solenoid was activated when the glass was in a less viscous state. I find using the delay mode help provide greater control of the taper length since you have more cooling and can effect the viscosity of the glass before it is pulled. The Sutter pipette cookbook is a great resource.

In addition, Denis Pare recommended the book "Advanced micropipette techniques". He advises “there is no better way to learn about intracellular recordings than to read early scientific papers. Read the papers by R. Llinas that were published in the late 70"s and 80s.”

Chapter 2

Spike timing amplifies the effect of electric fields on neurons: implications for endogenous field-effects

2.1.0 Abstract

Despite compelling phenomenological evidence that small electric fields (<5 mV/mm) can affect brain function, a quantitative and experimentally verified theory is currently lacking. Here we demonstrate a novel mechanism by which the non-linear properties of single neurons 'amplify' the effect of small electric fields: when concurrent to supra-threshold synaptic input, small electric fields can have significant effects on spike timing. For low-frequency fields our theory predicts a linear dependency of spike timing changes on field strength. For high-frequency fields (relative to the synaptic input), the theory predicts coherent firing; with mean firing phase and coherence each increasing monotonically with field strength. Importantly, in both cases, the effects of fields on spike timing are amplified with decreasing synaptic input slope and increased cell susceptibility (mV membrane polarization per field amplitude). We confirmed these predictions experimentally using CA1 hippocampal neurons *in vitro* exposed to static (DC) and oscillating (AC) uniform electric fields. In addition, we develop a robust method to quantify cell susceptibility using spike timing. Our results provide a precise mechanism for a functional role of endogenous field oscillations (e.g. gamma) in brain function, and introduce a framework for considering the effects of environmental fields and design of low-intensity therapeutic neuro-stimulation technologies.

2.2.0 Background and Significance

The study of how small electric fields affect brain function is important for several reasons. First, these studies provide insight into the mechanisms by which endogenous electric fields generated by the brain itself (e.g. delta, theta, gamma) could 'feed-back' unto the brain (Lutz et al. 2001, Parra and Bikson, 2004; Schaefer et al., 2006). Second, these studies address concerns about human exposure to environmental electro-magnetic fields (Hamblin 2002; Jefferys et al. 2003). Lastly, they have practical applications in the design of low-intensity brain stimulation treatments for neurological diseases (Ghai et al., 2000; Francis et al., 2003; Webster et al., 2006).

Small electric fields will polarize neurons by only a small amount; for this reason small electric fields have previously been suggested to have no physiologically relevant effects. However, the hypothesis that small felds can affect brain function has garnered support from phenomenological studies applying low-intensity electrical stimulation to brain slices (Ghai et al., 2000; Francis et al., 2003; Bikson et al., 2004) and humans (Marshall et al., 2006; Webster et al., 2006), the latter indeed showing a causal effect on slow wave oscillations and declarative memory. A quantitative and experimentally verified explanation for these findings has previously been lacking.

While neurons often encode information in their firing rate, the timing of individual action potentials (temporal coding) has also been shown to carry significant information (de Ruyter et al., 1997). Cortical neurons have been identified that fire with an accuracy of a few milliseconds in response to sensory stimuli (Mainen and Sejnowski, 1996; Trussel, 1999; Kara et al. 2000; Reinagel and Reid, 2000; DeWeese et al., 2003), in synchrony with overt behavior (Riehle et al., 2000), and in phase with ongoing *extracellular potential* oscillations (Kashiwandi et al., 1999;

Mehta et al., 2002; Harris et al., 2003).

Here we consider how small electric fields, which are in themselves not sufficient to trigger or suppress action potential activation in response to synaptic input, may nonetheless have an effect on neuronal information processing through induced changes in spike *timing*. Specifically, given a steady firing threshold and knowing that a membrane polarizes linearly with field strength (where the proportionality constant represents the susceptibility of the membrane potential to extracellular fields; Bikson et al., 2004), we make a number of quantitative predictions on the effects of extracellular fields on a neuron's spike timing: (1) For relatively low-frequency or DC fields, spike timing advances linearly with increasingly depolarizing field strength; (2) Oscillating fields promote coherent firing with the mean phase of firing falling within < 1/4 of the oscillatory cycle (on the positive rising edge); (3) Time advancement, phase delay, and coherence strength all increase with field strength amplified by membrane susceptibility and the inverse synaptic ramp slope. These quantitative predictions are validated here for hippocampal CA1 neurons *in vitro*. In addition, we develop a method to determine membrane susceptibility based on spike timing measurements. Taken together, this work yields the first quantitative framework for evaluating the effect of sub-threshold fields, with arbitrary (non-uniform) spatio-temporal waveform, on neuronal spike timing.

2.3.0 Methods

Transverse hippocampal slices (350 μm) were prepared from male Sprague-Dawley rats (125–150 g); anaesthetized and killed by cervical dislocation. The slices were stored in a holding chamber. After >60 min, slices were transferred to an interface recording chamber at 33°C.

Uniform electric fields were generated between two parallel Ag/AgCl electrodes (Ghai et al., 2000; Bikson et al., 2004) placed on the surface of the ACSF in the interface chamber; the wires were parallel to the direction of perfusate flow, 12 mm long and 10 mm apart. Field intensities were generated by a Power 1401 ADC/DAC (Cambridge Electronic Design, Cambridge, UK) and converted to a constant current by a stimulus isolation unit (2200, A-M Systems, Carlsborg, WA, USA). The polarity convention used refers to the anode on the Alveus side of the hippocampus.

Conventional recording techniques were used to measure activity from the CA1 pyramidal cell region. Intracellular electrodes (40–120 MΩ, pulled on a P-97; Sutter Instruments, Novato, CA, USA) were filled with 3M potassium chloride. Pyramidal neurons with an input resistance > 15.4 MΩ, resting membrane potential < -53.5 mV, over-shooting action potentials, and no spontaneous action potentials were accepted. Cell input resistance was monitored with a -0.3 nA current step. The voltage recorded by a field electrode (placed within 50 μm of the impaled neuron) was subtracted from the intracellular potential to obtain the transmembrane voltage and (partially) compensate for the exogenous potential artifact. For DC electric field experiments, no holding current was used. For AC electric field experiments, holding current (< -0.3 nA) was modulated to stabilize the resting membrane potential (RMP).

Depolarizing intracellular current ramps (0.1-1.6 nA/s) were generated and triggered to halt

<100 ms after action potential detection. The initiation of subsequent current ramps was intercalated by an eight second delay. The experimental paradigm consisted of interlacing control (no field) ramp trials with ramps applied during field application. Extracellular field application was initiated 400 ms before activation of depolarizing intracellular current ramps. Alternate DC polarity fields or alternate 30 Hz AC fields shifted 1/60 ms (180°) were tested, at varied peak field strengths (mV/mm). AC stimulation also included interleaved DC field and control trials as required to determine membrane susceptibility (see results).

Unless otherwise stated, all results are reported as means ± S.D.; n = number of cells. For resolution of lower-limit (<5 mV/mm) DC field effects, a paired t-test was performed for each cell at a single field magnitude by averaging time to first spike of neighboring control trials and pairing this with interlaced field trials (i.e. control / field / control), positive and negative fields were grouped due to field-effect symmetry resulting in 44-160 trials per neuron. For AC fields, phase-shifted trials of a single magnitude were combined (by subtracting 180° from one) resulting in 11-164 trials per neuron and field condition. The phase of the first spike relative to the applied field was determined. Mean firing phase, Φ, and vector strength, r, were computed from the population vector, which is defined as, $\vec{r} = \int d\varphi \; p(\varphi)\, \vec{r}_0(\varphi)$, with $\vec{r}_0(\varphi) = [\cos\varphi, \sin\varphi]$, and $p(\varphi)$ is the distribution of phases. This population vector can be estimated from the observed phases φ_i as the sample average, $\vec{r} = \frac{1}{N}\sum_{i=1}^{N} \vec{r}_0(\varphi_i)$. Linear regression was used to model the dependence of mean phase and coherence on field strength coefficient. Residuals from the regression line were used as criterion for outlier rejection based on inter-quartile range. (Moore et al., 1999).

2.4.0 Results

The single neuron amplification mechanism was validated using hippocampal CA1 pyramidal neurons *in vitro*. We first confirmed that firing time in response to injected depolarizing current ramps varies linearly with incremental polarization and in proportion to the inverse of ramp slope. We then demonstrated that timing changes in direct response to applied uniform DC fields follow the same linear properties. These timing changes were used to derive membrane polarization susceptibility. Finally, we confirmed the predicated effects of AC fields (in the gamma frequency range) on firing coherence and phase. Portions of this work have been previously presented in preliminary form (Radman et al., 2006).

2.4.1 Firing time changes linearly with increasing polarization

Assuming a constant firing threshold one would expect that an incremental polarization ΔV, which is applied with a voltage ramp, $\dot{V} = dV / dt$, should lead to a time advancement of: $\Delta t = \Delta V / \dot{V}$, where Δt is the firing time of control minus the field stimulus condition. Hyper-polarization of CA1 pyramidal neurons, with an increasingly negative DC holding current, ΔI, incrementally delayed action potential firing time in response to an intracellular current ramp, $\dot{I}$. (Linear current ramps lead to linear voltage ramps if the change is sufficiently slow – here 0.1-1.6 nA/s). Importantly, for the conditions tested here, action potential threshold did not vary with ramp slope or polarization in agreement with previous findings (Fricker et al., 1999). The change in timing increased linearly with the holding current, and inversely proportional to ramp slope (Fig. 2.1; n=12 cells, $R^2 > 0.95$ for linear regressions).

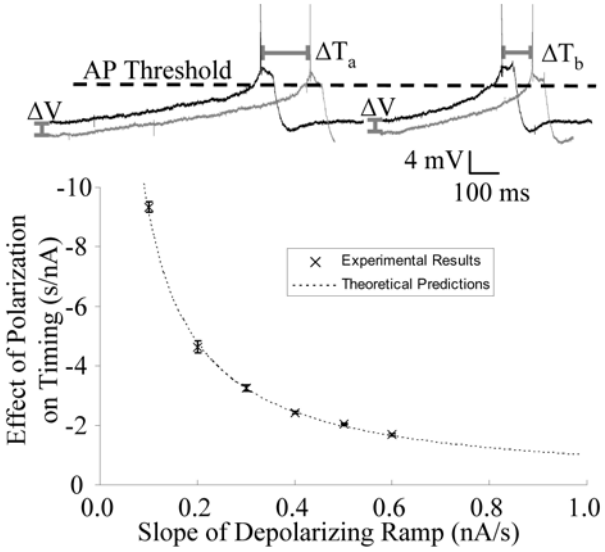

Figure 2.1. CA1 pyramidal cell response to depolarizing current ramps. Top: Intracellular recording of the response to a 0.4 nA/s (left) and 0.7 nA/s (right) intracellular current ramp (action potentials clipped). In both cases hyperpolarization (ΔV) delayed the AP firing time. The change (ΔT), is inversely proportional to depolarizing ramp slope, ΔT_a:ΔT_b as 1/0.4:1/0.7. Bottom: The inverse relationship between the ramp slope and the sensitivity to membrane polarization due to negative DC holding current can be summarized in a single plot. Experimental results ("x") fit directly to the theoretical prediction of a inverse slope. Error bars represent standard error of the slope of a linear regression line fitting holding current (nA) versus AP timing (s) data (n ≥ 7 for linear regression data).

These results show that the membrane dynamics of real CA1 pyramidal neurons support the single neuron amplification mechanism hypothesized (R is membrane resistance):

$$\Delta t = \frac{\Delta I}{\dot{I}} = \frac{R\Delta I}{R\dot{I}} = \frac{\Delta V}{\dot{V}} \ . \qquad (Eq.\ 1)$$

2.4.2 Spike time advances with increasing applied DC electric fields

Uniform DC electric fields were generated across hippocampal slices while synaptic input was simulated by injecting a current ramp. Constant uniform fields induced a membrane

polarization; consistent with previous reports (Chan et al., 1986; Bikson et al., 2004), the magnitude of the somatic polarization was a linear function of field strength and the polarity was dependent on the direction of the field (not shown). Applied fields could significantly modulate the firing latency of single neurons resulting from intracellular depolarizing ramp current injection. DC fields inducing membrane hyperpolarization delayed action potential initiation while fields inducing membrane depolarization had the opposite effect (Fig. 2.2A; n=8). For each injected ramp slope, the experimental data could be fit with a regression line (r^2 = 0.90 ± .1); the slope of this fit indicated the change in timing induced per mV/mm applied electric field (in s/mV·mm^{-1}). As intracellular ramp slope decreased, the fit timing sensitivity to applied fields (s/ mV·mm^{-1}) linearly increased, supporting our prediction of an inverse relationship. This inverse relationship is summarized for 3 cells in Figure 1.2B where for each cell the changes in time per electric field ($\Delta t / E$) is plotted against the corresponding injected ramp slope ($\dot{V}$).

The somatic polarization induced by an electric field is set by the cell-specific membrane susceptibility constant *c, ΔV=cE.* Membrane susceptibility can be determined using timing data by extension of (*Eq.* 1): $c = \dot{V}\Delta t / E$ (see also *Eq.* 2 in discussion). Susceptibility may thus be calculated from a single timing change measurement at one field amplitude, using a single intracellular ramp slope. A more robust method involves using the inverse relationship in Fig 1.2B to simultaneously fit all data from a single cell. Indeed, for each cell, these plots are well approximated by the curve, $y = cx^{-1}$, (r^2 > 0.98, $y = \Delta t / E$, $x = \dot{V}$) where *c* indicates the estimated membrane susceptibility. Using this indicator, we determined polarization susceptibilities of c = 0.11 ± 0.05 mV/mV·mm^{-1} (*n* =10). Using a conventional method (Bikson et al., 2004) consisting of recording the intracellular potential and subtracting the measured

stimulation 'artifact' at a second iso-potential electrode, the polarization induced per electric field was 0.13 ± 0.14 mV/mV·mm^{-1} (n = 9).

Figure 2.2. Effects of applied extracellular DC electric fields on CA1 pyramidal neuron firing time in response to intracellular depolarizing ramp slopes. A, Positive (hyper-polarizing) fields delayed action potential initiation while negative (depolarizing) fields expedited AP onset. Note that for each ramp slope series, the relationship between firing time (Δt) and applied field amplitude is linear. Moreover, the slope of this relationship varies inversely with the slope of the injected intracellular ramp (i.e. 10.1:12.7:15.2 as 1/.017:1/.015:1/.012). The injected current ramp slope (.4, .5, .6 nA/s) translated to voltage slope by cell resistance (25.3 MΩ for this cell). The change in timing for any given field is 'amplified' as the slope of the ramp is decreased. Reported: mean +/- SD (r^2 > .94, p <.01 for the three regressions shown here). B, The relationship between ramp slope and timing change per field magnitude is plotted for 3 cells. Each line in Fig. 2.2A corresponds to a point of the "Cell 3" series shown (vertical error bars show standard error of the slope, horizontal show SEM). Data for each cell is fit with y=c/x (r^2 > .98, p < .01 for all regressions shown). Legend shows membrane susceptibility , c, in units of mV/mV·mm^{-1} (y·x or s/mv·mm^{-1}·mV/s).

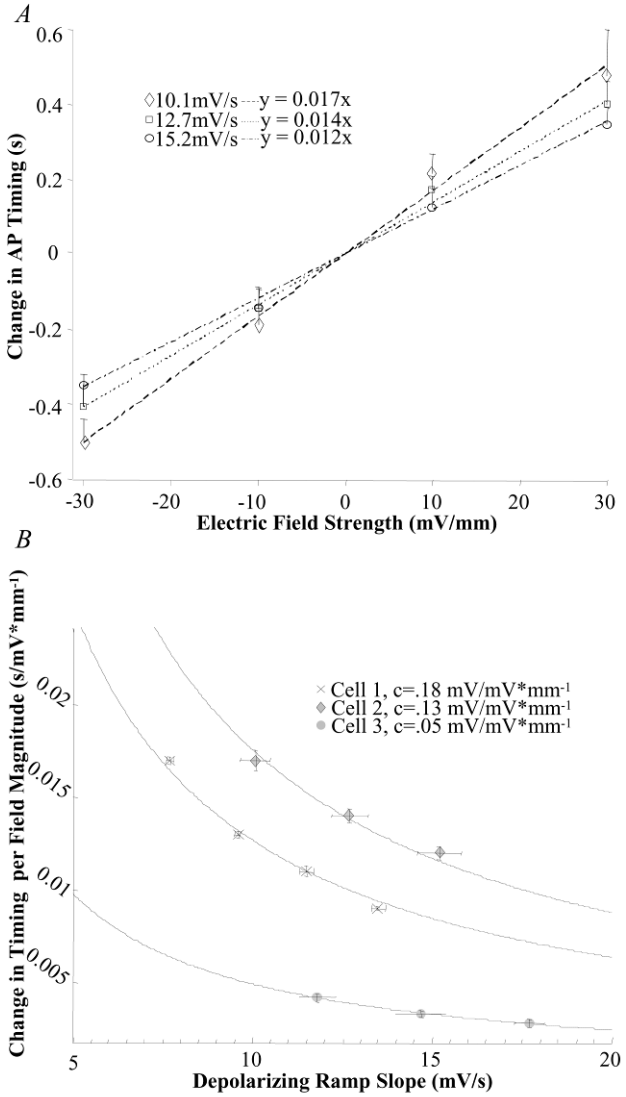

2.4.3 Resolution of lower-limit DC effects

For a 0.4 nA/s injected current ramp, we observed a significant change in timing induced by ± 1 mV/mm DC field strengths (n = 4). The average change in timing observed was 11 ± 5 ms (mean ± SEM). Assuming a susceptibility of 0.11 mV per 1 mV/mm applied field and a 12 mV/s voltage ramp (induced by a 0.4 nA/s current injection into an ~30 MΩ cell resistance), a

change in timing of ~9 ms would be expected.

For 0.5 mV/mm DC fields and a 0.4 nA/s current ramp, a statistically significant change in timing was observed in 1 of 4 neurons tested. For the cell showing a significant change, the average change in timing observed was 8 ± 3 ms (mean ± SEM), while 4.5 ms was the predicted change (as above).

In attempts to resolve significant timing changes due to .5 mV/mm DC electric fields, we could reject the null hypothesis of a sample mean different than zero in 1 out of 4 attempts. For our experimental paradigm, the standard deviation of the difference between time to action potential under a 0.5 mV/mm field and a control trial was 54 ms for 0.4 nA/s current injections. If this standard deviation remained stable over time, we would need > 500 tests to resolve the predicted 4.5 ms difference induced by a 0.5 mV/mm field in 50% of neurons tested. Conversely, our attempts to resolve the effects of .5 mV/mm fields with < 160 trials leads to a power of a < 80% chance to reject an effect when it is really there (Type II, β error); indeed, we rejected 75% of our attempts. For the predicted timing change in response to a 1 mV/mm field, we would expect to detect a significant change in 83% of our attempts (< 160 trials); we resolved all four neurons. We note that the limits to resolve a field-induced change are determined by the noise (experimental and biological) in spike timing and subsequent effect on the repeats necessary to reach statistical significance; the latter is limited by duration of neuronal impalement integrity.

2.4.4 Uniform AC electric fields induce spike coherence

Uniform AC electric fields were generated across hippocampal slices and the firing time in

response to an intracellular depolarizing ramp monitored. The frequency (30 Hz) and slope of the ramp (72 ± 22 mV/s) were selected to mimic extracellular gamma oscillations and synaptic theta depolarization (Harris et al., 2002) typical for theta-modulated gamma activity (Chrobak et al., 2000, Fischer et al., 2002). Significant coherence of the firing time with the applied field oscillation was observed in 21 of 29 field conditions (Rayleigh test, $p<0.02$) including fields as low as 1mV/mm. Mean firing phase was analyzed for 19 field conditions (excluding two outliers, see methods). During application of fields, neuron coherence (as measured by the Rayleigh vector strength) increased with the mean firing phase falling approximately within 1/4 of the oscillatory cycle (40^o – 110^o, Fig. 2.3). For each cell, the coherence and mean phase were plotted against the field amplitude applied to that cell (in mV/mm) times the individual cell susceptibility (determined as above using interleaved DC stimulation trials) and divided by the current-induced voltage ramp slope and field period (i.e. $cE(\dot{V}T)^{-1}$; see discussion); the resulting plots (Figure 3C) show significant correlation with this characteristic parameter (phase, $p<0.02$; coherence, $p<0.002$).

Figure 2.3. Effects of applied extracellular AC electric fields on CA1 pyramidal neuron firing time in response to intracellular depolarizing ramp slope. A, Overdrawn intracellular recordings in response to an injected current ramp with accompanying circular scatter plot. Top traces and circular plot: in the absence of uniform AC electric field (control), spike traces show low coherence and insignificant (random) mean angle. For circular scatter plots, outer edge shows individual spike phase φ, direction of arrow on inset shows mean angle, Φ, length of arrow shows coherence as measured by vector strength, r, with perfect coherence reaching edge of inset. Lower traces and plot: middle trace shows overdrawn samples in the presence of a 10 mV/mm uniform 30 Hz AC electric field (stimulus), bottom trace in the presence of a 10 mV/mm uniform 30 Hz AC electric field phase shifted 180 degrees from previous (stimulus). Lower circular scatter plot combining field-present cases (by shifting data of bottom-left case back 180 degrees), arrow shows increased coherence with a mean firing phase at ~π/2, on the rising edge of electric field oscillation. *B,* Theoretical predictions of AP phase response to injected current ramp

under AC electric field. Top: dashed line shows simulated membrane voltage with same control condition as in experiment *"A"*. Black trace shows the simulated membrane response under field stimulus condition as in *"A"*. If the previous cycle did not cross threshold, the membrane will not increase to a greater value during the red region on the phase axis. The cell is thus constrained to fire in the "unvisited" voltages (green), in this case on the positive rising field edge quadrant (<π/2). Bottom: predicted distribution of spike timing phase; the inset shows the resulting circular plot of this distribution with mean angle and vector strength. Assuming a delay, α, between the extracellular field and induced membrane polarization, the dashed arrow shows the mean firing phase relative to the extracellular field; note similarity to experimental results in "*A*". *C,* Experimental results of mean phase and coherence vector strength. Horizontal axes is given by the experimentally observed value of $\frac{cE}{\dot{V}T}$ (see discussion). The dashed green lines indicate the field positive rising edge quadrant shifted by an estimated α=40° membrane phase delay (see discussion). Error bars show SEM.

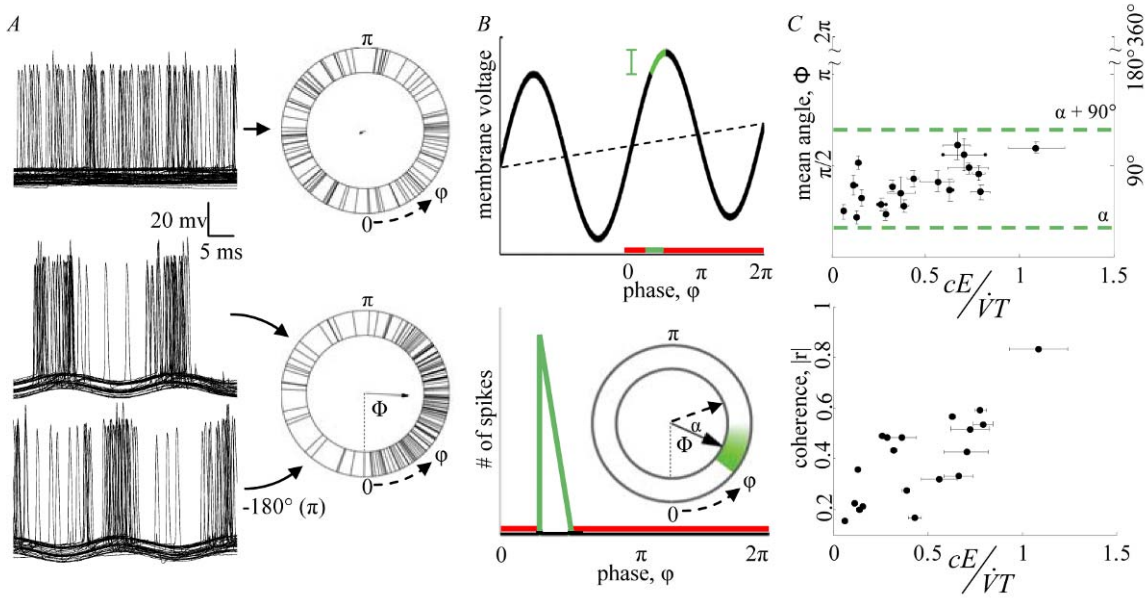

2.5.0 Discussion

2.5.1 Predictions of timing changes

Despite mounting phenomenological evidence that small fields can entrain network activity, and have an effect on brain function, to date, there is no experimentally verified mechanistic theory on how this causal interaction may occur. We hypothesized that incremental polarization due to an extracellular field will affect the time of threshold crossing; under the assumption of a constant firing threshold we made a number of predictions that will now be described.

For the case of low-frequency or DC extracellular fields with strength *E*, which polarize a cell by, $\Delta V_E = cE$, where *c* is the susceptibility of the membrane to an extracellular field, we predicted an advance in spike timing of:

$$\Delta t = \frac{\Delta V_E}{\dot{V}_I} = \frac{cE}{\dot{V}_I} \qquad (Eq.\ 2)$$

Note that *c* refers to the susceptibility effective at the site of spike *initiation* (i.e. the soma). Subscripts emphasize that ΔV_E results from application of the extracellular field, while $\dot{V}_I$ is the result of a concurrent intracellular/synaptic current ramp which induces the action potential spike.

For the case of AC fields, we predicted increased coherence of spiking with the ongoing oscillations. Change in coherence can be quantified as a change in the distribution of firing times

occurring at phase φ within the oscillatory cycle (with duration *T*). The distribution of firing phase, $p(\varphi)$, for the present experimental preparation can be expressed as:

$$p(\varphi) \propto \frac{1}{2\pi} + \frac{1}{T}\frac{cE}{\dot{V}_1}\cos(\varphi + \alpha) \qquad \textit{(Eq. 3)}$$

assuming that φ is within a depolarizing phase of the membrane oscillation, and the cell has not yet fired (green shaded region in Fig. 2.3B), otherwise, $p(\varphi) = 0$, since only the time to the first spike was analyzed in the experiment (red shaded region). *Eq. 3* assumes a uniform initial distribution and no noise (see supplementary material, Radman et al. 2007, for derivation). Because the membrane acts as a low pass-filter, a delay between the extracellular field and the induced transmembrane polarization phase is expected; this is expressed in *Eq. 3* as phase delay, α. The phase distribution of *Eq. 3* can be characterized by the mean phase, Φ, and the vector strength, r, as shown in Fig. 2.3C. Both should increase monotonically with $cE/\dot{V}$, with mean phase remaining constrained to the range, $\alpha \le \Phi \le \alpha + 90^o$.

This series of predictions were born out under the experimental conditions tested.

For both, DC and AC fields, the strength of the effect on spike timing scales with:

$$\frac{cE}{\dot{V}} = GE \qquad \textit{(Eq. 4)}$$

where, $G = c/\dot{V}$, can be considered as a timing amplification factor. It increases with the susceptibility of the membrane to extracellular polarization (mV of transmembrane polarization at the site of action potential initiation per mV/mm extracellular field) and decreases with the depolarizing synaptic ramp slope (in mV/s). For the case of AC fields, the timing amplification factor is further scaled by field frequency (*1/T*).

2.5.2 Generalization and Quantitative parameterization

Equations 2 through 4 provide a general theoretical framework for considering the effects of any electric field on spike timing in any neuron with appropriate membrane dynamics (see below). Quantitative application requires knowledge of the intracellular (ramp slope) and extracellular (field amplitude and period) waveforms, which are readily measured. For low-frequency (quasi-static) fields, cell susceptibility can be determined using the method outlined above.

Equation 3 can be readily applied to any periodic field with a complex spatio-temporal profile, by considering only the maximum positive instantaneous *cE* (the phase in the field cycle when the induced transmembrane depolarization is maximal). The susceptibility, *c,* is specific to a given spatio-temporal waveform (e.g. frequency, non-uniformity). The uniform field susceptibility, for any given temporal waveform, presumably sets a *lower* susceptibility bound for non-uniform fields. The membrane, acting as a low-pass field filter (Bikson et al., 2004), may introduce a frequency-specific phase delay $\alpha > 0^o$, as well as an attenuated (relative to DC) susceptibility. The DC field susceptibility thus sets an upper limit for AC fields of *comparable spatial profile.* The phase delay may be estimated assuming the membrane acts as a first-order low pass filter; thus a membrane time constant of τ= 30 ms should result in a phase delay of $\alpha \approx 40^o$ for 30 Hz fields, consistent with our experimental findings using timing data (Fig. 2.3).

2.5.3 Applying timing changes to discern susceptibility

As reinforced above, the polarization susceptibility of neurons is of fundamental importance in

assessing subsequent effects on nervous system function. The field induced polarization is inherently variable between neurons due in part to alignment with the field, neuronal geometry, and membrane biophysical properties (Rattay, 1998). Here we developed a method utilizing measured timing changes, to calculate the sensitivity of the neuron to polarization by an electric field (Fig. 2.2B). This technique may yield greater accuracy in measuring polarization sensitivity to small (<5 mV/mm) electric fields than can be achieved by conventional methods. Conventional methods are limited because experimental (line) noise is of magnitude comparable to the polarization induced by small fields and they require an additional, precisely positioned, iso-potential field electrode. Our timing-based method may be readily applied for non-uniform fields (e.g. unipolar, bipolar, DBS spatial waveforms) and *in vivo*. As a further advantage, our timing method may inherently extract the susceptibility at the spike initiation zone. Conventional polarization measurements here and previously (Bikson et al, 2004), show average susceptibility (coupling-constant) values similar to our method utilizing timing changes.

2.5.4 Membrane Dynamics and Noise

The theory developed here assumes a simple threshold mechanism equivalent to an integrate-and-fire model neuron with constant firing threshold. The accuracy of the assumption of constant threshold depends on a number of factors including the channel kinetics of the specific cell type and the nature of the incoming synaptic input; experimental and theoretical work show both dynamic and constant thresholds (Fricker et al. 1999; Azous and Gray 2000). The present experiments with DC stimulation controlled for potential slope-dependent thresholds by measuring only changes in timing relative to a control condition with the same ramp slope.

The experimental data for the AC stimulation is generally consistent with a constant threshold.

Interestingly, our theory on the scaling of timing effects with ramp slope also explains a number of existing observations on the timing jitter that results from synaptic and membrane noise. If noise induces variability in the membrane potential (ΔV_n) we expect the resulting spike timing jitter will scale with, $\Delta t = \Delta V_n / \dot{V}$. Indeed, under frozen noise stimulation, precise spike timing is observed (Bryant and Segundo 1976) with a timing precision that increases for faster stimuli (Mainen and Sejnowski, 1995). Corresponding simulations with a Hodgkin-Huxley neuron subject to membrane noise also show that increased stimulus magnitude increases timing precision (Schneidman 1998). A similar inverse dependence of spike time precision with stimulus intensity can be observed in cortical pyramidal neurons subject to synaptic noise (Shu et al. 2003). According to our theory, both a reduced time constant, as well as an increased magnitude of the stimulus, will increase membrane ramp slope and thus reduce timing jitter due to noise.

2.5.5 Functional Amplification – Network Consequences

We found that a 1 mV/mm uniform field induced in average a transmembrane potential change of ~0.1mV. Compared to the scale of depolarization necessary to bring a neuron from rest to threshold (~15mV), these fields were previously considered insignificant with respect to action potential initiation. Previous action potential threshold studies identified changes due to electric fields of less than 5 mV/mm (Jefferys et al., 1981). Rather than spike generation, here we demonstrated changes in timing, consistent with the proposed amplification mechanism. The present results provide a potential mechanism for the effects on network spike timing previously

demonstrated *in vitro* with exogenous uniform fields as low as 0.1 mV/mm (Deans et al., 2003; Francis et al., 2003; Fujisawa et al., 2004) and *in vivo* with calculated fields of 1.2 mV/mm (Marshall, 2006).

Electric field induced changes in spike timing would be particularly relevant for temporal coding during coherent (synchronous) network activity. For example, theta-modulated gamma activity in the hippocampus has been identified as a physiological correlate for a number of phenomena including spatial navigation, memory, etc. (Miller, 1991; Kahana et al., 2001; Canolty et al., 2006). Extracellular gamma activity amplitudes of up to 0.2 mV are observed *in vivo* (Csicsvari 2003) and *in vitro* (Hajos 2004, Mann 2004) with complete phase reversal across 100 μm (from stratum pyramidale to stratum radiatum) resulting in field gradients of 4 mV/mm. An estimated gamma-field induced polarization of at least $\Delta V_E = 0.4$ mV (uniform field sensitivity providing a lower-bound for the coupling factor) is small compared to the full scale voltage fluctuations (e.g. AP threshold); however considering a theta oscillation synaptic ramp with slope of $\dot{V}_I = 0.2$ mV/ms (15 mV change between resting and firing potentials within 75 ms of a half a theta cycle), a time shift of $\Delta t = 1\,\text{ms}$, and a Rayleigh vector strength, a measure of circular coherence, of $r = 0.39$ with a mean angle of α, can be estimated. Thus extracellular fields oscillating at gamma frequency may have a functional effect on AP timing during theta activity even in a single cycle. Moreover, since gamma field activity is coherent across several mm of the pyramidal layer (Csicsvari et al., 2003; Mann et al., 2004), extracellular gamma oscillations could facilitate coherence across a large population of neurons. Finally, computational studies have demonstrated that an additional synchronizing effect may result during recurrent network activity when small changes in time add up over multiple cycles (Parra

and Bikson, 2004).

The discussion above assumes that the timing of extracellular fields relative to synaptic input acts to promote coherent firing by advancing late spikes and delaying early spikes. However, a different temporal relationship between fields and underlying network activity could also have the opposite effect of advancing early spikes and delaying late spikes thus acting as a safety mechanism to prevent hyper-synchronization.

Our approach for predicting field-induced timing changes (*Eq. 2, 3*) can be readily extended to other networks using readily measurable extracellular and intracellular waveforms and using either field susceptibility estimates or our novel method to measure susceptibility. Indeed, extracellular field oscillations are a ubiquitous marker for network oscillations (Chrobak et al., 1998; Donoghue et al. 1998, Csicsvari, 2003; Nunez and Srinivasan, 2005; Sarnthein et al., 2007). More than an epiphenomenon, our results indicate a functional role for field potentials in modulating spike timing. Indeed, the information content of endogenous extracellular potentials oscillations is often comparable to multi-unit activity (e.g. Scherberger et al., 2005, Heldman and Wang, 2006, Liu and Newsome, 2006). Synaptic mechanisms underlie the generation of many classes of oscillations (Bragin et al., 1995; McBain et al. 1999;Buzsaki et al., 2003; Jones and Wilson, 2005; Siapas et al., 2005; Netoff et al., 2005); field-effect coupling is not proposed as alternative, but rather as a complementary mechanism with unique spatio-temporal features.

Our system does not presuppose the source, exogenous or endogenous, of the modulating electric fields. Thus, the equations developed in this paper can be similarly applied in predicting the effects of environmental electric fields; EMF safety standards have not previously considered

effects of timing. Finally, our results support the development of therapeutic stimulation technologies targeting neuronal timing; abnormal timing is indeed a hallmark of many neurological disorders and sub-threshold stimulation approaches may be readily adapted for non-invasive (transcranial) technologies.

Chapter 3

Role of Cortical Cell Type and Morphology in Sub- and Suprathreshold Uniform Electric Field Stimulation

3.1.0 Abstract

The neocortex is the most common target of sub-dural electrotherapy and non-invasive brain stimulation modalities including transcranial magnetic stimulation (TMS) and transcranial current simulation (TCS). Specific neuronal elements targeted by cortical stimulation are considered to underlie therapeutic effects, but the exact cell-type(s) affected by these methods remains poorly understood.

We determined if neuronal morphology or cell type predicted responses to sub- and suprathreshold uniform electric fields. We characterized the effects of sub- and supra-threshold electrical stimulation on identified cortical neurons *in vitro*. Uniform electric fields were applied to rat motor cortex brain slices, while recording from interneurons and pyramidal cells across cortical layers, using whole cell patch clamp. Neuron morphology was reconstructed following intracellular dialysis of biocytin. Based solely on volume-weighted morphology, we developed a parsimonious model of neuronal soma polarization by sub-threshold electric fields.

We found that neuronal morphology correlated with somatic sub-threshold polarization. Based on neuronal morphology, we predict layer V pyramidal neuronal soma to be the most sensitive to polarization by optimally oriented sub-threshold fields. Supra-threshold electric field action potential threshold was shown to reflect both direct cell polarization and synaptic (network) activation. Layer V/VI neuron absolute electric field action potential thresholds were

lower than Layer II/III pyramidal neurons and interneurons. Compared to somatic current injection, electric fields promoted burst firing and modulated action potential firing times.

3.2.0 Background and Significance

Clinical application of transcranial magnetic stimulation (TMS) and transcranial current stimulation (TCS, encompassing transcranial direct current stimulation (tDCS), cranial electrotherapy stimulation, transcranial electric stimulation (TES), and electroconvulsive therapy) are promising non-invasive approaches for the treatment of a number of psychiatric, neurological, and pain disorders (George et al., 1999; Avery et al., 2006; Boggio et al., 2006; Fregni et al., 2006; Liebetanz et al., 2006; Webster et al., 2006) as well as the study of human cognitive function and neural plasticity (Uy and Ridding, 2003; Kincses et al., 2004; Fregni et al., 2005; Marshall et al., 2006). Because the electric field (voltage gradient) in the extracellular space induced in the brain by TMS/TCS decays with distance from the stimulating coil or electrode, the neocortex is the most common target of non-invasive electrotherapy (Amassian et al., 1992; Wassermann et al., 1996; Krings et al., 1997; Miranda et al., 2006; Komssi et al., 2007). Invasive cortical stimulation using sub-dural strips/arrays is indicated for a range of therapeutic and diagnostic applications including pain and pre-operative brain mapping (Normann et al., 1999; Badi et al., 2002).

Fundamental questions remain regarding the cellular targets of each cortical stimulation paradigm, including the relative activation of morphologically and functionally diverse groups of inhibitory interneurons and excitatory pyramidal cells (Esser et al., 2005). Stimulation waveform, direction, and frequency is thought to preferentially affect specific cortical cell types (Pascual-Leone et al., 1994; Takano et al., 2004; Esser et al., 2005) and/or specific segments of a

neuron such as axonal bends and terminations (Amassian et al., 1992; Maccabee et al., 1993; Amassian et al., 1994). Neuronal segments oriented toward the stimulating anode (virtual anode for electric fields induced by TMS (Amassian et al., 1994)) have been shown to hyperpolarize, and concomitantly the segments oriented toward the (virtual) cathode depolarize (Fig. 3.1) (Hern et al., 1962; Chan et al., 1988).

The effects of electric field-induced polarization has traditionally been categorized as "subthreshold" changes in ongoing neuronal processing/timing (Purpura and McMurtry, 1965; Chan and Nicholson, 1986; Bikson et al., 2004), or "suprathreshold" stimulation that directly triggers action potentials (Ranck, 1975; Chan and Nicholson, 1986; Lopez et al., 1991). Clinical brain stimulation modalities, and associated therapeutic outcomes, may depend specifically on subthreshold (e.g. tDCS) and/or suprathreshold (e.g. TMS) neuronal effects (see (Wagner et al., 2007a) for review). Cortical cell types (Gatter et al., 1978) , distinguished by their laminar position, network connectivity, and neuronal morphology/biophysics, play defined roles in network processing and thus merit investigation in the context of both sub- and suprathreshold stimulation paradigms (Esser et al., 2005).

In response to the unique electric fields induced by each brain stimulation modality (Amassian et al., 1994; Miranda et al., 2003; Wagner et al., 2007b; Datta et al., 2008), neuronal membranes are considered to polarize in a "compartment" specific manner; the polarized compartments interact according to the electrotonic decay along the neuron (Figure 2.1). Neuronal modeling (Hause, 1975; Tranchina and Nicholson, 1986; Rattay, 1989; Nagarajan et al., 1993) and *in vitro* (Svirskis et al., 1997; Bikson et al., 2004) studies of electric field stimulation have identified morphological features which govern the polarization of (interacting)

neuronal compartments, including branching patterns and membrane space constants. Changes of compartment angle relative to an applied electric field (e.g. activating function, the 2nd derivative of the extracellular voltage along the neuronal membrane), branch terminations, or changes in inter-compartment impedance can determine the locations of entry and exit of induced transmembrane currents that lead to polarization (Tranchina and Nicholson, 1986; Rattay, 1989; Maccabee et al., 1993; McIntyre and Grill, 1999; Bikson et al., 2004). The neuronal space constants (λ), and related diameter of axons and dendrites, govern the axial distribution of these induced transmembrane polarizations, and therefore regulate the degree to which neuronal compartments interact (Tranchina and Nicholson, 1986; Plonsey and Altman, 1988; Svirskis et al., 1997; Plonsey and Barr, 1998). Concurrent polarization of individual segments of a neuronal tree can lead to complex changes in overall neuronal function by modulating cellular biophysics (Valero-Cabre et al., 2005; Rotem and Moses, 2008) including non-linear voltage-gated conductances, synaptic efficacy, and AP threshold or timing (Ranck, 1975; Chan et al., 1988; Lopez et al., 1991; Roth, 1994; Durand, 2001).

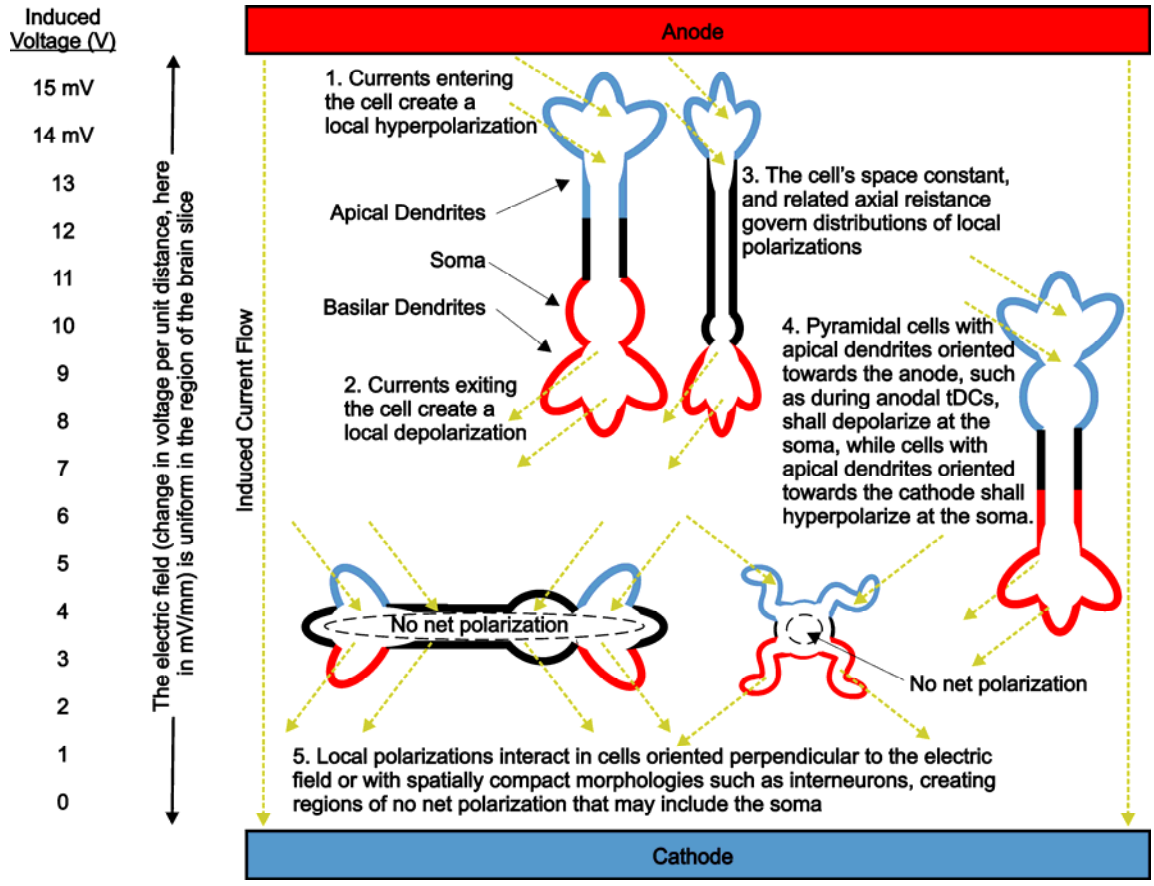

Figure 3.1: Schematic of cortical neuron polarization by uniform DC electric field stimulation. A constant current is applied between the parallel Ag/AgCl wires (Red Bar: Anode, Blue Bar: Cathode). The induced currents across a homogenous resistivity, creates a uniform voltage gradient between the Anode and Cathode. The electric field is the first spatial derivative of the voltage gradient (left two columns). Because the field is uniform, the absolute position of a neuron between the Anode and Cathode does not matter. 1,2) As current passes in, through, and out the neuron, the neuronal membrane is polarized in a compartment specific manner (Blue membrane: Induced hyper-polarization; Red membrane: Induced depolarization). 3) The cell membrane biophysics and cell morphology relative to the electric field determine the distribution of the induced polarization. 4) The relative position of the soma in the dendrite tree determine if it is depolarized or hyper-polarized by a given direction electric field. 5) Certain morphologies may result in the cell not being polarized, even as dendrite compartment are polarized by electric fields.

The goal of the present study was to determine if the distinct morphological features of cortical cell types affect their response to stimulation by electric field. We performed whole-cell recordings, of pyramidal cells and interneurons in rat motor cortex brain slices, during uniform

electric field stimulation *in vitro*. Morphological reconstructions of biocytin-filled neurons were correlated with electrophysiological responses to electric fields. We considered differences between cortical cell types in their response to both subthreshold and suprathreshold stimulation. These data were used to consider the cellular targets of clinical cranial stimulation therapies.

3.3.0 Methods

3.3.1: Brain Slice Preparation. Coronal slices (300 μm) of primary motor cortex (M1) were prepared from male P21-25 rats. In brief, rats were anaesthetized with intraperitoneal ketamine (7.4 mg/kg) and xylazine (0.7 mg/kg) and euthanized by decapitation. Following decapitation, the brain was quickly removed, blocked, and placed into ice-cold (4°C) oxygenated artificial cerebral spinal fluid (ACSF) prior to the previously described slicing procedure.

In some experiments, the glutamatergic transmission blockers CNQX (AMPA receptor antagonist, 20 μM) and APV (NMDA receptor antagonist, 50 μM) were added to the perfusate (Sigma-Aldrich, St. Louis, MO).

3.3.2: Whole cell patch clamp recording and data acquisition. Conventional whole-cell patch clamp recording techniques were used to measure activity from neurons in M1. Neurons were visualized with IR-DIC illumination (Olympus BX51WI, Center Valley, PA, USA), and identified according to layer and gross morphology. Patch pipettes (~4-7 MΩ tip resistance) were pulled on a Flaming/Brown microelectrode puller (P-97, Sutter Instruments, Novato, CA, USA). Pipettes were filled with (in mM) 120 KGlu, 10 NaCl, 20 KCl, 10 HEPES, 2 Mg-ATP, 0.3 Na-GTP, 0.5 EGTA, and 0.3-1% biocytin (wt/vol) for subsequent visualization of the neurons. Upon obtaining a high resistance seal (> 1 GΩ) with a neuron but prior to establishing whole-cell configuration, the microscope objective (water immersion; 40x, Olympus) was removed from the bath to reduce perfusate level (and related electric field) non-uniformities. Once a stable whole-cell configuration was obtained (resting membrane potential of <-55 mV, overshooting action potentials, generation of repetitive action potentials in response to a depolarizing current pulse),

neurons were classified according to discharge pattern in response to a constant depolarizing current pulse (100 ms) as intrinsically bursting, regular spiking, etc. (McCormick et al., 1985; Yang et al., 1996; Brumberg et al., 2000).

3.3.3 Generation of uniform electric fields and quantification of neuronal response. Uniform electric fields were generated across individual slices; the wires were parallel to the direction of perfusate flow and measuring 15-16 mm long and 7-9 mm apart. Field waveforms were generated by a Power 1401 ADC/DAC (Cambridge Electronic Design, Cambridge, UK) and converted to a controlled current source by up to three parallel stimulus isolation units (2200, 2300, A-M Systems, Carlsborg, WA, USA). Due to the reduced current density caused by the deeper fluid levels in submerged patch recording chambers, to achieve electric field magnitudes comparable to those applied in previous studies utilizing interface recording chambers (Bikson et al., 2004; Radman et al., 2007), an order of magnitude greater current intensity was necessary. This, in turn, limited the maximum electric field applied (for example in determining action potential thresholds). The convention of electric field polarity used in the present report refers to the anode on the pial side of the cortex.

Post-hoc corrections for voltage differences between the field and intracellular electrode (measured at the termination of each recording) were made by scaling the electric field command waveform to the inter-electrode difference and subtracting from the recorded transmembrane voltage. We note that this creates a residual onset-and offset artifact that was not included in our analysis. For each cell, the somatic steady-state transmembrane voltage response to ~ 5 mV/mm electric field steps (Fig. 3.2B), up to ~ +/-30 mV/mm, were linearly fit (Fig. 3.2C), the slope of

which determined the cell-specific subthreshold somatic polarization per unit electric field applied (Fig. 3.3), in units of mV of polarization per mV/mm of electric field (mV*(mV/mm)$^{-1}$). This slope, which has also been referred to here as "mV per mV/mm", and previously as "coupling coefficient" and "cell susceptibility" (Bikson et al., 2004; Deans et al., 2007; Radman et al., 2007), reduces to mm, and shall be referred to here as polarization length, λ_p.

Suprathreshold electric fields induced non-linear polarizations with characteristic excitatory post-synaptic potential (EPSP) waveforms (Ramos et al., 2008a) and/or action potentials, as determined by visual inspection. Averages are reported as mean +/- standard error. Statistics within a 95% confidence interval have been labeled as significant.

Figure 3.2. Sub-threshold electric fields polarize cortical neuronal soma linearly. *A,* Example morphological reconstruction of a LV pyramidal neuron (black), and LV fast-spiking interneuron (red) *B,* Incrementing electric field steps of 5.8 mV/mm (bottom) linearly polarize cell soma (top). Reconstructions shown are from LV regular spiking pyramidal neuron of *A* (top). *C,* Summary of the polarization per electric field for the neurons shown in *A*. The slope of the fitted line determines the sub-threshold field polarization sensitivity, λ_p, for each neuron. LV pyramidal neuron (black) = .27 mV*(mV/mm)$^{-1}$, LV fast-spiking interneuron (red) = -.02 mV*(mV/mm)$^{-1}$.

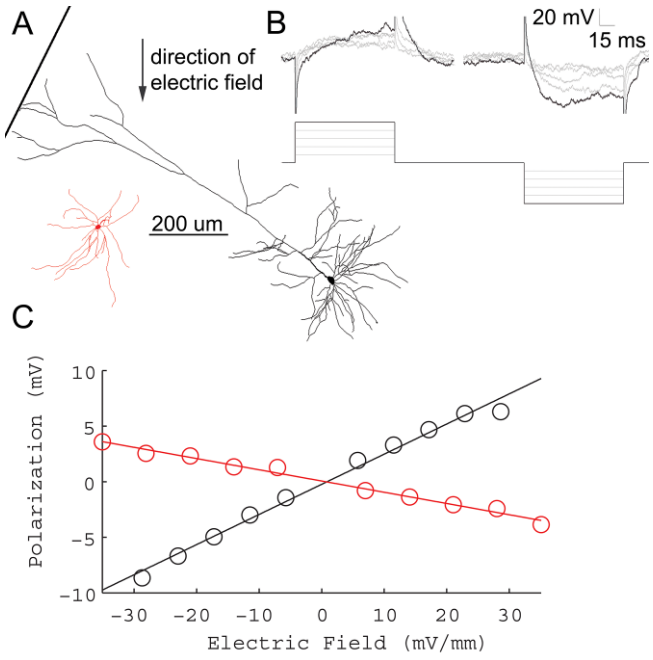

3.3.4: Morphological reconstruction of biocytin-filled neurons. Following recordings, slices were placed in cold fixative (4% paraformaldehyde in 0.1 M phosphate buffer) and kept at 4°C for no more than 2 weeks. Biotin-avidin-HRP histochemistry was performed as previously described (Brumberg et al., 2003; Rocco and Brumberg, 2007; Ramos et al., 2008b). Briefly, sections were first placed in 1% H_2O_2/0.5% MEOH in phosphate buffer saline (PBS) in order to quench endogenous peroxidase activity. After 3 washes in PBS, sections were permeabilized for one hour in PBS containing 0.2% Triton-X (Sigma, St. Louis, MO, USA). Sections were then placed in an avidin-HRP mixture (ABC Kit, Vector Labs, Burlingame, CA, USA) for 2 hrs. Following 3 washes in PBS, sections were reacted in 0.05% diaminobenzidine/0.015% H_2O_2. Slices were washed in PBS, mounted onto gelatin coated-slides and coverslipped in DPX (Electron Microscopy Sciences, Hatfield, PA, USA). For three-dimensional morphological

reconstructions, the Neurolucida system (MicroBrightfield, Williston, VT, USA) was used in conjunction with an Olympus BX51 microscope using 4x (0.1 numerical aperture (NA)), 10x (0.4 NA) and 60x (1.4 NA, oil) objectives. Digital images were taken using an Optronics Microfire camera (Optronics Inc., Muskogee, OK, USA). Morphological measurements were made using the NeuroExplorer software package (MicroBrightfield, Williston, VT, USA). Dendritic morphology was used to indentify cell type and layer. The tracing was aligned so the direction of the electric field traversed along the 90° line from the top of the tracing to the bottom. NeuroExplorer branched structure analyses were used to measure segment angle (φ_{seg}) and volume information for each segment of each individual neuron's tracing.

3.3.5: Volume-weighted polar histogram generation. The volume of each segment was binned by segment angle in a polar histogram (Fig. 3.5A-C), and summarized by a single vector of mean angle (degrees) and vector length (volume, μm^3). 90 degrees is defined as pointing towards the anodal electric field stimulating electrode (Fig. 3.5A-C. Histograms were generated using the Matlab (Mathworks, Natick, MA, USA) Circular Statistics Toolbox by Philip Berens.

3.3.6: DC stimulation strength-time to first spike curves. To determine respective stimulation "DC-chronaxies", the threshold stimulation magnitude in response to incrementing electric field steps of 100 ms duration (functionally DC), as well as to incrementing 100 ms steps of somatic current injection, was plotted against the inverse of the time to first spike. These data were fit to the equation $S=S_o+ S_o C/t$, where S is the threshold stimulation magnitude (in nA for current injection, mV/mm for electric field stimulation), S_o is the rheobase corresponding to the

horizontal asymptote of the strength-duration curve, *C* is the DC-chronaxie equal to the duration of stimulation pulse having twice the intensity of the rheobase, and *t* is time to first spike in milliseconds (Nowak and Bullier, 1998). Note "classic" strength duration curves are determined using duration of incrementing stimulation pulse necessary to trigger an action potential (Bostock, 1983).

3.4.0: Results

We quantified the acute effects of uniform electric fields on cortical neurons *in vitro*. For the cases of sub-threshold and suprathreshold fields we considered if neuronal responses could be distinguished based on cortical cell type or neuronal morphology. Cortical cell types can be defined by anatomical and biophysical distinctions, while we developed a parsimonious metric of neuronal morphology relative to the orientation of applied uniform fields. In response to subthreshold fields, neuronal compartments polarize linearly with the amplitude of the applied electric field (Tranchina and Nicholson, 1986; Plonsey and Altman, 1988; Rattay, 1989; Plonsey and Barr, 1998; McIntyre and Grill, 1999); for each neuron, somatic sub-threshold sensitivity is defined by the polarization length constant: λ_p (in mm). Thus, for a given subthreshold electric field E (in mV/mm), neuronal soma will polarize $E \bullet \lambda_p$ mV. The sign of the polarization length reflects the polarity of polarization for a given electric field direction. Suprathreshold fields induce non-linear responses in the cell membrane including action potentials and/or EPSPs from activated afferents. The electric field threshold for triggering an action potential in a given neuron reflects the neuron's specific sensitivity to suprathreshold fields. The main objective of this study was to determine if sub- and suprathreshold sensitivities to electric fields could be correlated with cortical cell type or neuronal morphology.

3.4.1: Cortical cell subthreshold polarization in response to uniform electric fields

A total of 51 neurons from M1 were recorded, 37 of which were identified by cortical layer and cell type. Consistent with findings in other structures (Chan et al., 1988; Bikson et al., 2004), the direction of cortical sub-threshold somatic polarization increased linearly with

increasing electric field steps, and reversed polarity with the direction of the applied electric field. Per our convention (see Methods), a 'positive' sub-threshold soma polarization indicated a positive field (anode proximal to pial surface) resulting in membrane depolarization; while a 'negative' sub-threshold polarization indicates a positive field resulting in a membrane hyper-polarization The polarity and polarization length (sensitivity) of each neuronal soma in response to an applied electric field was quantified.

51 cells had a subthreshold transmembrane polarization length, λ_p, ranging from -.29 to .49 mm (such that field-induced subthreshold polarization = λ_p*E mV, where E is the applied electric field in units of mV/mm). 14 identified layer V/VI (LV/VI) pyramidal cells had a range of polarization lengths, λ_p, from -.03 to .49 mm. The 8 identified layer II/III (LII/III) cells had subthreshold polarization lengths, ranging from -0.05 to 0.13 mm. 15 identified interneurons (from across all layers), had subthreshold polarization lengths ranging from -.29 to .14 mm. These data are thus indicative of the range of possible sub-threshold polarization values for a distributed population of cortical neurons. These polarization ranges are reported without accounting for variable cell angle relative to the electric field, and morphology differences within and across cell types (McCormick et al., 1985; Meyer, 1987) (including slicing related damage).

Without accounting for variable cell morphology relative to the electric field, a significant difference was found between the polarization length, λ_p , for interneurons across layers and LV/VI pyramidal neurons ($p < .02$), the difference between interneurons across layers and LII/III pyramidal neurons approached significance ($p = .06$)) (T-test, Fig. 3.3). Layer V neurons represented the represented the seven highest (19%) individual somatic polarization values of the 37 identified cells, and were on average significantly higher values than L2/3

pyramidal neurons and interneurons across layers after rejecting cells damaged due to slicing (marked with an "x" in Fig. 3.3).

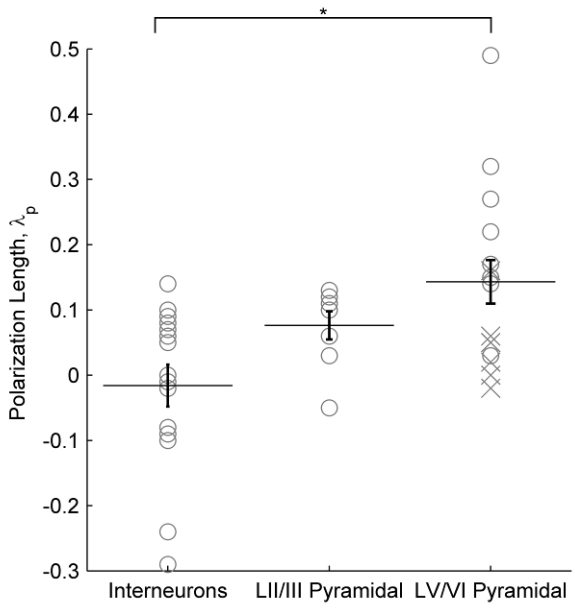

Figure 3.3: Cortical cell type polarization sensitivity. The polarization length, λ_p (mm), an indicator of mV or polarization per unit electric field applied (mV/mm), is shown according to cell type. Asterisk denotes significant difference (T-test) found between LV/VI pyramidal neurons and interneurons across layers. Points labeled as an "X" are neurons with cut dendritic trees that have still been included in all analyses. Error bars represent the standard error of the mean.

Figure 3.4 (below). Cortical neuron morphological reconstructions in decreasing order of electric field induced somatic subthreshold polarization sensitivity. 3 items are listed for each cell, electric field induced somatic polarization length, λ_p (mm), an indicator of mV of polarization per unit electric field applied (mV/mm); layer and cell type (pyramidal or interneuron); and if tested for that cell, electric field induced firing threshold. An asterisk next to the label for cell type denotes a neuron with a presumably cut dendritic tree (slicing related damage), that has still been included in all analyses.

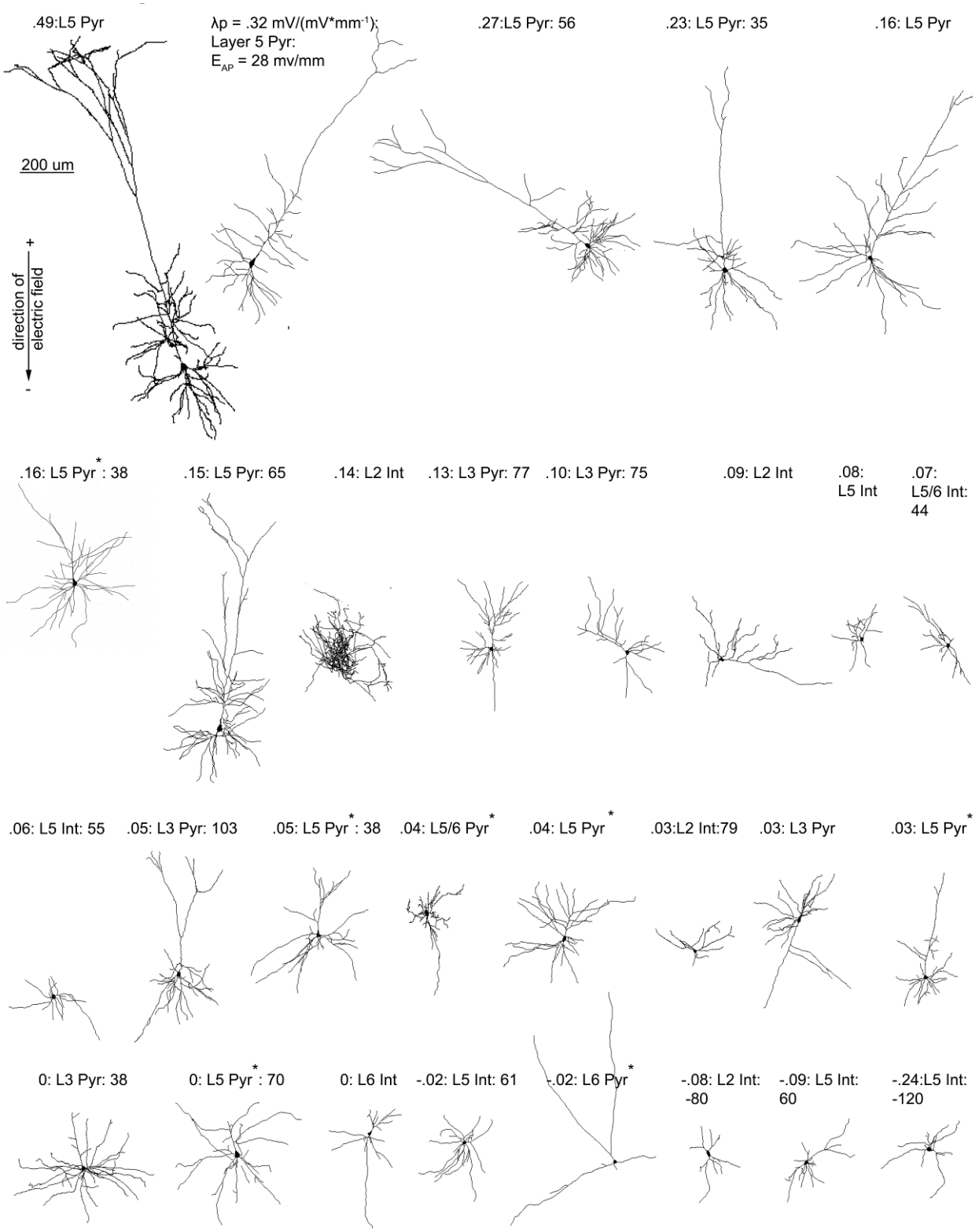
.49:L5 Pyr
λp = .32 mV/(mV*mm-1);
Layer 5 Pyr:
EAP = 28 mv/mm
.27:L5 Pyr: 56
.23: L5 Pyr: 35
.16: L5 Pyr
200 um
direction of electric field
+
-
.16: L5 Pyr* : 38
.15: L5 Pyr: 65
.14: L2 Int
.13: L3 Pyr: 77
.10: L3 Pyr: 75
.09: L2 Int
.08: L5 Int
.07: L5/6 Int: 44
.06: L5 Int: 55
.05: L3 Pyr: 103
.05: L5 Pyr* : 38
.04: L5/6 Pyr*
.04: L5 Pyr*
.03:L2 Int:79
.03: L3 Pyr
.03: L5 Pyr*
0: L3 Pyr: 38
0: L5 Pyr* : 70
0: L6 Int
-.02: L5 Int: 61
-.02: L6 Pyr*
-.08: L2 Int: -80
-.09: L5 Int: 60
-.24:L5 Int: -120

3.4.2: Neuronal morphology relative to applied electric field correlates to induced subthreshold polarization: volume weighted polar histograms.

Volume weighted polar histograms were constructed based on morphological reconstructions of intracellularly recorded neurons (see methods). This reduced representation of individual neuron morphology may be described by a mean angle and vector length (Fig. 3.5A-C). Mean angle and vector length were significantly correlated to somatic polarization length, λ_p (Fig. 3.5D, Fig. 3.6, regression model: $\lambda_p = m$*sine(mean angle) * vector length, for each neurons means angle, vector length, and polarization length, where m represents a single scaling variable common to all neurons). The significantly fit plane illustrates the correlation between the asymmetry of neuronal morphology relative to the soma (vector length), modulated by the sine of the mean angle of that morphological projection relative to the electric field, with increasing polarization length (F-statistic=19.52, $p < .001$, $r^2 = .41$, $n = 30$). Neuronal morphologies with mean angles of 0 or 180° (i.e. perpendicular to the electric field) would be represented in the model with polarization lengths of 0 mm (sine(0˚) = sine(180°) = 0). Mean angles of 90° or 270° degrees would be represented as the optimal orientation relative to the electric field to respectively de- or hyperpolarize the neuron (sine(90°)=1, sine(270°)=-1). Electric field induced AP threshold did not correlate with mean angle and vector length for our sampled cortical neuron population.

Figure 3.5 (below). Polar histogram coherence vector: Neuronal morphology predicts somatic polarization sensitivity to sub-threshold electric fields. *A-C,* Example tracings and corresponding volume-weighted polar histograms of (*A)* LV regular spiking pyramidal neuron with electric field orientation. The polarization length, λ_p (mm), an indicator of mV of polarization per unit electric field applied (mV/mm), = .32 mm, the polar histogram can be summarized by the variables: mean angle = 46° and vector length = 47 um^3, representing the center of mass of the histogram; (*B)* LII fast spiking interneuron with polarization length = .14 mm, mean angle = 99° and vector length = 35 um^3; and (*C)* LV fast spiking interneuron with polarization length = -.02 mm, mean angle = -127° and vector length = 30 um^3. *D,* Summary plot of all neurons recorded and traced, with polar histogram coherence vectors as predictors of somatic polarization per electric field for each neuron. The colored plane is the statistically significant, best fit regression to the equation: polarization length = m*sine(mean angle)*vector length ($p < .02$, $r^2 = .41$, n=30).

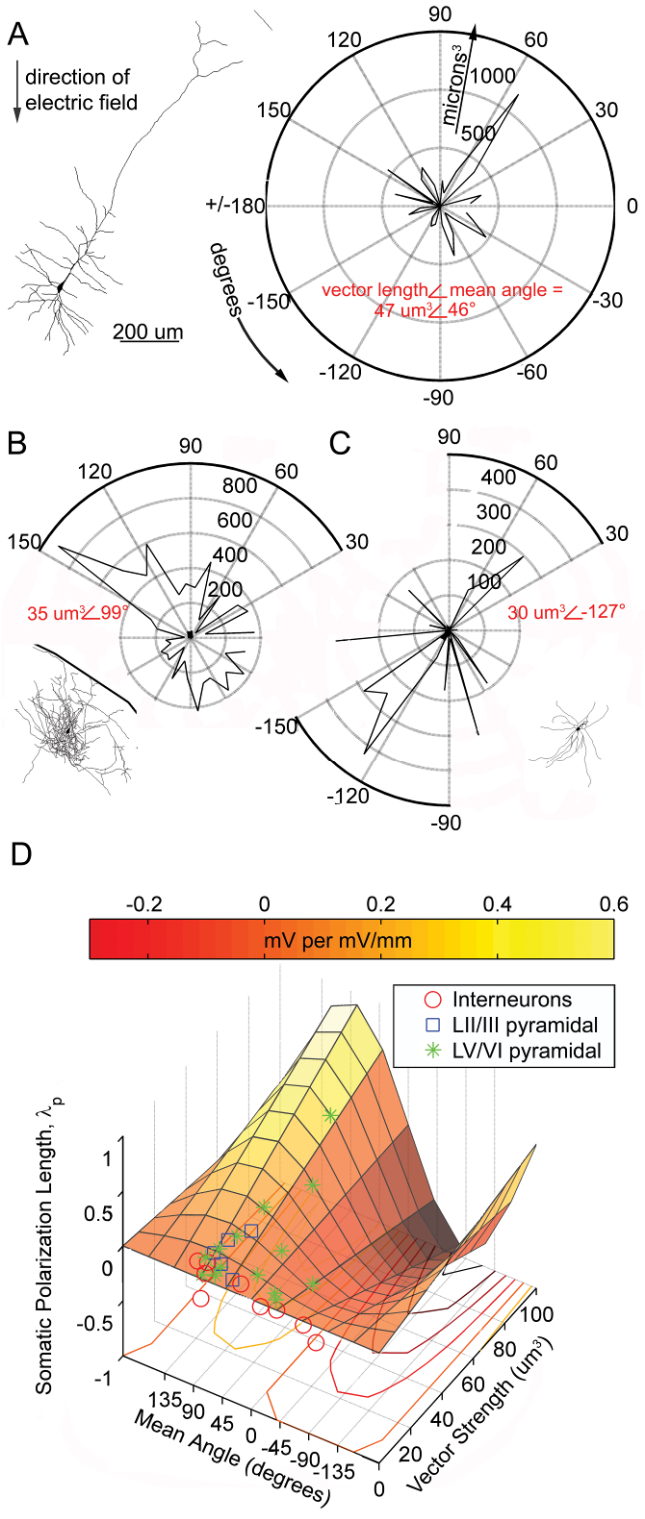
A
direction of
electric field
200 um
90
120
60
150
30
+/-180
0
-150
-30
-120
-60
-90
microns³
1000
500
degrees
vector length∠ mean angle =
47 um³∠ 46°
B
90
120
60
800
600
150
30
400
200
35 um³∠ 99°
C
90
400
60
300
30
200
100
30 um³∠ -127°
-150
-120
-90
D
-0.2
0
0.2
0.4
0.6
mV per mV/mm
Interneurons
LII/III pyramidal
LV/VI pyramidal
Somatic Polarization Length, λp
1
0.5
0
-0.5
-1
135
90
45
0
-45
-90
-135
Mean Angle (degrees)
0
20
40
60
80
100
Vector Strength (um³)

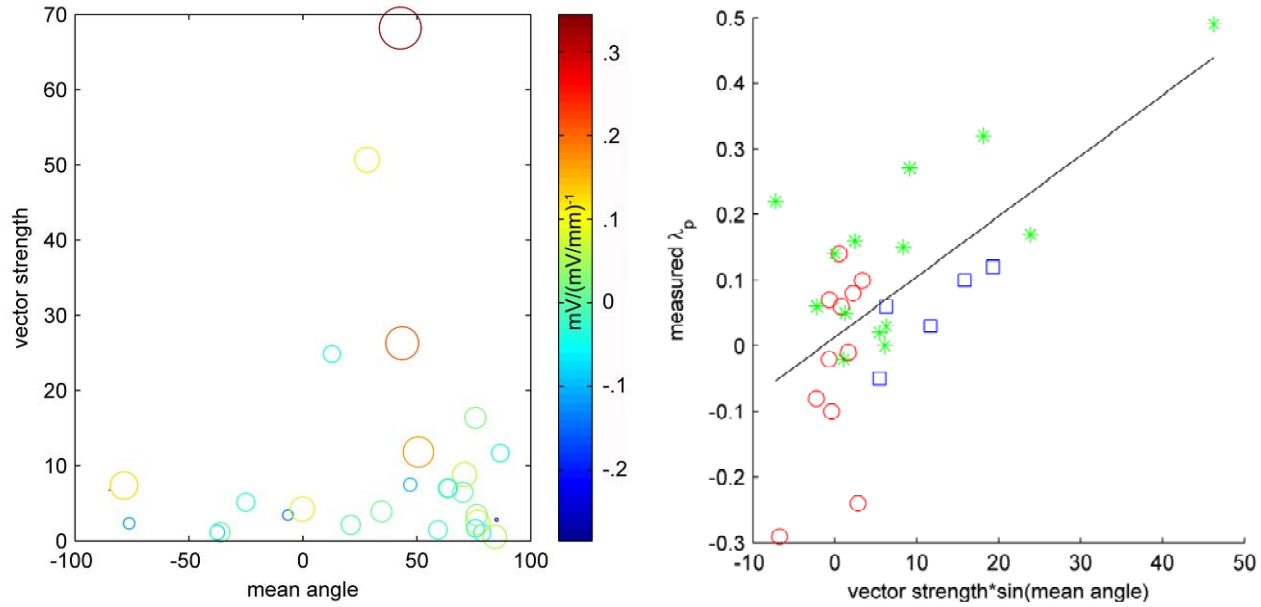

Figure 3.6: Polar histogram coherence vector: Neuronal morphology predicts somatic polarization sensitivity to sub-threshold electric fields. Summary plot of all neurons recorded and traced, with polar histogram coherence vectors as predictors of somatic polarization per electric field for each neuron. Left: Each cell's mean angle and vector length is indicated by it's location on the x and y-axis respectively. Polarization length is indicated by the color and size of the circle representing each cell. Right: The results of the polar histogram model for each cell: theoretical somatic polarization=vector strength*sin(mean angle) is plotted on the x-axis. Measured somatic polarization is plotted on the y-axis. Red circles represents interneurons, blue squares LII/III pyramidal, green stars LV/VI pyramidal.

If all the neurons we recorded were optimally oriented to the electric field (mean angle = 90°), the regression model would reduce to $\lambda_p \propto$ vector length. A significant difference was found between the vector length for interneurons and both LII/III pyramids ($p << .001$) as well as LV/VI pyramidal neurons ($p < .04$) across layers (T-test, Fig. 3.7).

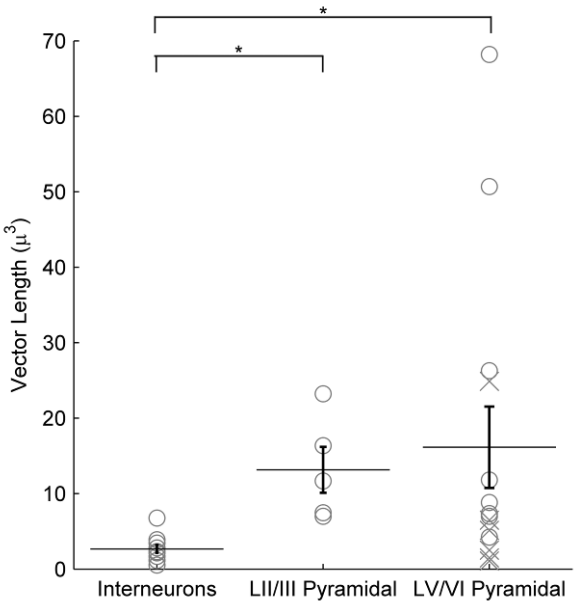

Figure 3.7. Cortical cell type vector lengths. The polar histogram (Fig. 3.6) summary variable vector length, is shown according to cell type. Asterisk denotes significant difference (T-test) found between as interneurons across layers and both LV/VI pyramidal neurons, and LII/III pyramidal neurons as well. Points labeled as an "X" are neurons with cut dendritic trees that have still been included in all analyses. Error bars represent the standard error of the mean.

3.4.3: Cortical cell AP threshold in response to uniform electric fields

The minimum action potential (AP) threshold in response to 100 ms, +/- polarity electric field square pulses was determined (n=26). 3 cells were able to fire in both electric field polarities and the lesser magnitude polarity was considered the "minimum" threshold. 18 of 26 cells had a positive minimum threshold ranging from 28 to 101 mV/mm (mean = 58 +/- 5 mV/mm), and 2 cells had negative minimum thresholds of -80 and -120 mV/mm (mean = -100 +/- 20 mV/mm). 6 cells did not fire an AP in response to the maximum electric field tested in

either polarity. No cells fired in response to the offset of the electric field step (e.g. in response to anodic break).

The minimum electric field induced firing threshold for identified LV/VI pyramidal cells ranged from 28 to 79 mV/mm (n=11, mean=57 +/- 6 mV/mm). For LII/III pyramidal neurons, the minimum electric field AP threshold range was 70 to 104 mV/mm (n=6, 80 +/- 3 mV/mm). Thus all identified pyramidal cells had a positive minimum AP threshold. The minimum electric field AP threshold range for interneurons was 44 to 79 mV/mm in the positive direction (n=6, 58 +/- 9 mV/mm), and -80 and -120 mV/mm in the negative direction (n=2, -100 +/- 20 mV/mm) (Fig. 3.9). A significant difference was found between the absolute value electric field firing threshold of LV/VI pyramidal neurons and LII/III pyramids ($p < .002$) (T-test, Fig. 3.8). Note this difference was observed without accounting for variable cell angle relative to the electric field, morphology differences within and across cell types (and slicing related damage), or pre-synaptic contribution.

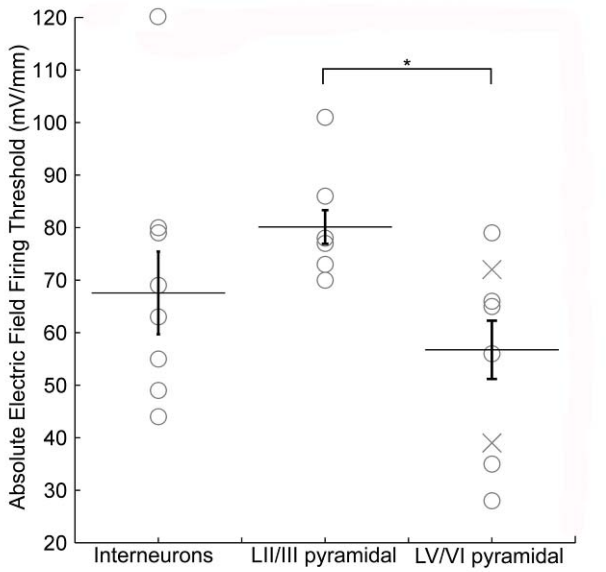

Figure 3.8. Cortical cell type electric field firing thresholds. The minimum absolute electric field firing threshold, in response to 100 ms incrementing electric field steps, is shown according to cell type. Asterisk denotes significant difference (T-test) found between LV/VI pyramidal neurons and LII/III pyramidal.

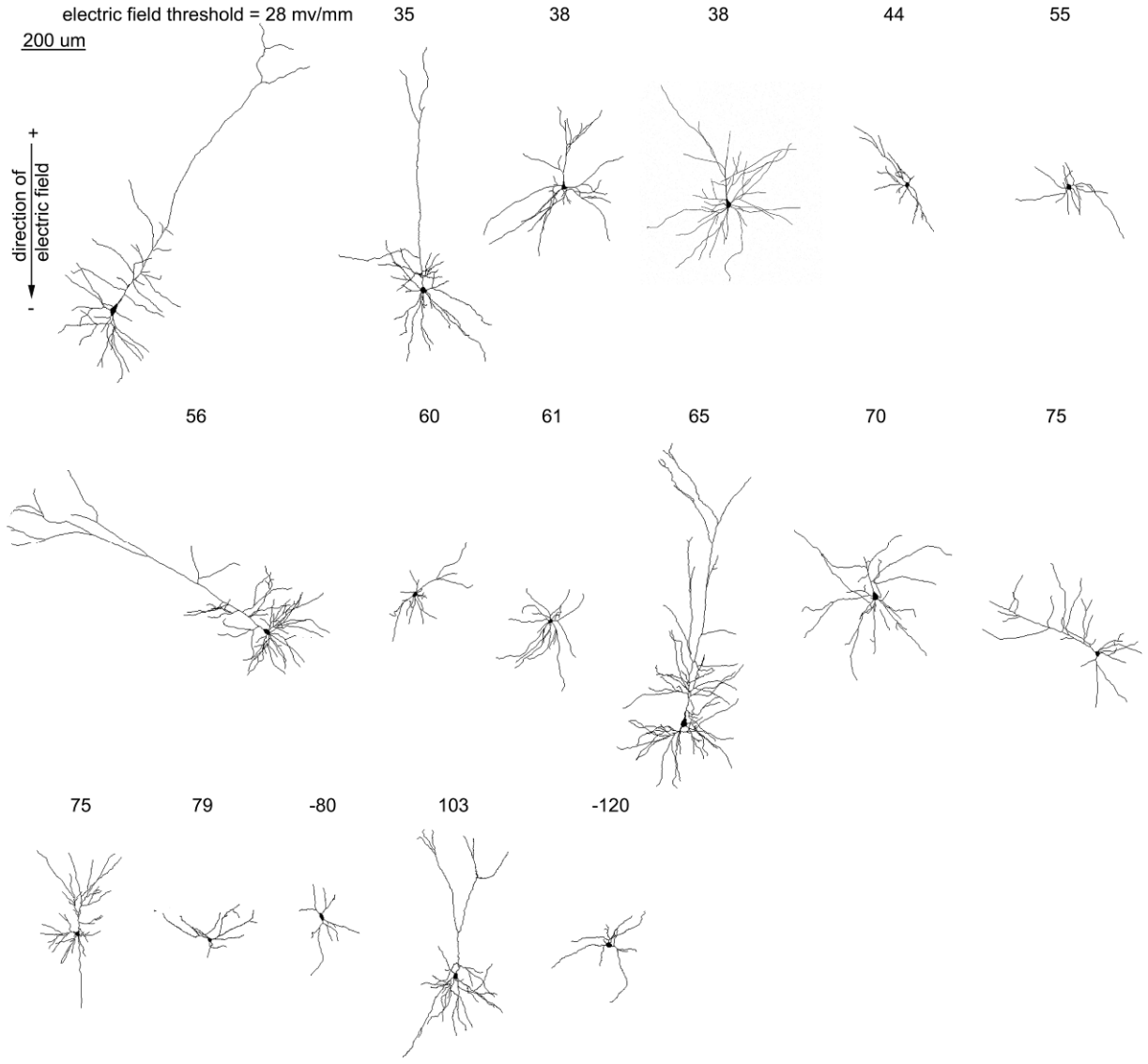

Figure 3.9. Cortical neuron morphological reconstructions in order of absolute value of electric field induced action potential threshold. Above each cell is listed electric field induced action potential threshold

Increasing intensity of electric field beyond the subthreshold polarization range (see methods) resulted in EPSPs for most cells (n=34) reflecting the activation of action potentials in axons afferent to the specific cortical neuron. This was in distinction to relatively rare EPSPs when electric field stimulation was off. In all but 3 of 26 suprathreshold responding neurons, EPSPs contributed to the depolarization towards AP threshold (Fig. 3.10). For cells exhibiting

EPSPs, the minimum positive electric field value inducing EPSPs ranged from 12 to 69 mV/mm (mean = 49 +/- 4 mV/mm) (n=18). The negative EPSP threshold range was -22 to -104 mV/mm (mean = -62 +/- 7) (n=16). These EPSPs were suppressed by bath application of glutamatergic transmission blockers CNQX and APV (n=4, Fig. 3.10) consistent with an orthodromic origin. After glutamatergic transmission blockade, action potentials could no longer be triggered in these four cells when stimulated up to the maximal intensity electric field tested (from +/- 79 to 110 mV/mm across these four cells). This analysis underscores the potential contribution of afferent glutamatergic synapses in depolarizing cells to AP threshold, in response to 100 ms electric field pulses.

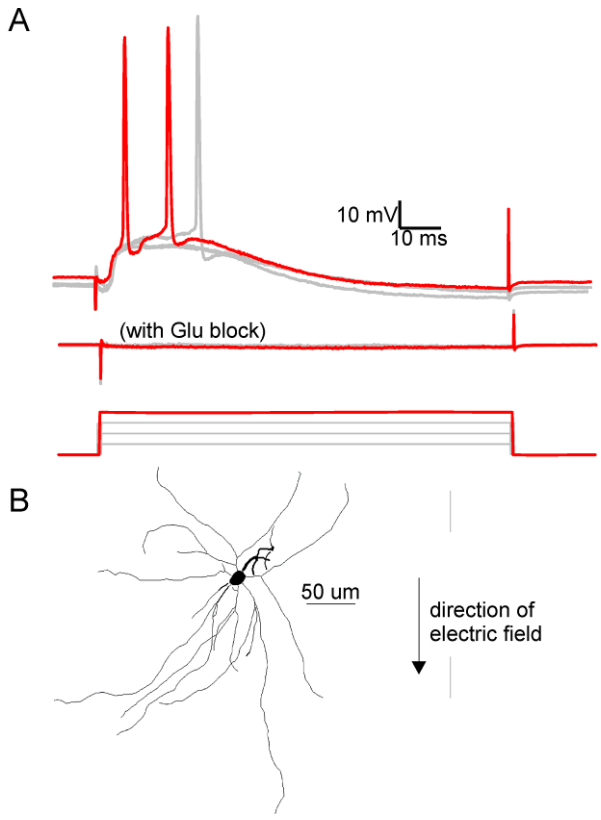

Figure 3.10. Electric field induced EPSPs are reduced by bath application of CNQX and APV. ***A,*** **Overlay of the response to electric field steps of increasing intensity.** ***Top*****: Recorded intracellular voltage response to electric field steps of 51, 57, 63, and 70 (red trace) mV/mm. Note 63 and 70 mV/mm electric field steps induced action potentials.** ***Middle*****: Voltage response to the same field intensities after 15 minute bath application of 20 μM CNQX and 50 μM APV.** ***Bottom:*** **Applied electric field waveforms.** ***B,*** **Tracing of LV fast-spiking interneuron described in *A*.**

Stimulation parameters used in TMS and TES are typically short duration pulses less than 1 ms, and can be either monophasic or biphasic. As an initial characterization of the biophysics of cortical cell types in response to stimuli of brief duration, we tested the response of 19 cells to (0.5 ms square wave electric field stimuli up to the intensity limits of our experimental set-up (ranging from up to 79 to 120 mV/mm). 2 of 19 cells responded to a 0.5 ms square pulse step

(mean 88 +/- 8 mV/mm); these cells responded to this 0.5 ms electric field stimuli with a spike ~2 ms after stimulation onset; this short delay is indicative of direct neuronal activation (i.e. the time course excludes synaptic contributions). EPSPs, reflecting orthodromic activation, were observed in another 2 cells at the maximum intensity tested (mean 100 +/- 6 mV/mm). Thus, as expected, cortical AP threshold increases rapidly with decreasing pulse duration (see also DC-chronaxie below); We can conclude that electric field strengths greater than 79 to 120 mV/mm are necessary for significant activation of *quiescent* (see discussion) cortical neurons in slice preparations by 0.5 ms (TMS-like) electric field pulses.

3.4.4: Differing mechanisms of action potential initiation between intracellular current injection and suprathreshold electric field stimulation.

In 10 of 26 cells, we observed a transition from regular spiking behavior in response to intracellular current injection, to intrinsic burst spiking (see methods) when the same cell is stimulated by an electric field (Fig. 3.11A). 4 of these cells were classified as LII/III pyramidal and 6 were classified as LV/VI pyramidal. This data indicates a change in the intrinsic firing pattern of cells, depending on the type of stimulation used.

The firing time of 26 cells in response to 100 ms incrementing steps of electric field and somatic current injection was compared. DC stimulation intensity-time to first AP plots (e.g. strength-duration curves) were constructed for each cell (see Methods), for both stimulation types (Fig. 3.11A). In 23 out of 26 cells, the DC-chronaxie through electric field stimulation was lower then that of intracellular current injection, resulting in a significant difference between stimulation types (t-test, $p < .01$, Fig. 3.11B). 8 of these cells were unable to be indentified as a

particular cell type. Among LV/VI cells, a significant difference between the DC-chronaxie of electric field stimulation and that of intracellular current injection was evident (n=8, $p < .001$), while for LII/III cells (n=6, $p = .09$) and for interneurons ($p=.07$, n=4) the difference approached significance.

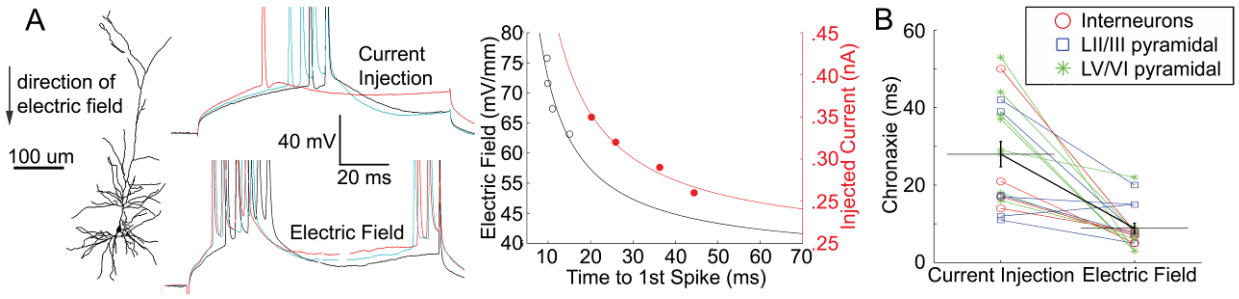

Figure 3.11: Time to 1st spike-strength of stimulation chronaxie measurements are lower for electric field stimulation than somatic intracellular current injection. *A,* Example morphological reconstruction of a L5 intrinsic bursting pyramidal neuron with transmembrane polarization in response to successive steps of intracellular current injection (top), and electric field stimulation (bottom). Note modulation of firing pattern from regular spiking (top, current injection), to intrinsic bursting (bottom, field stimulation). Summary plot (right), of the time to first spike in response to electric field stimulation (left axis, black) and injected current (right axis, red). The solid lines are best fit curves to y=1/(time to first spike). *B,* Comparison of chronaxies, for current injection and electric field stimulation, for each recorded neuron. Statistically significant difference ($p < .01$) between stimulation methods for all cells.

3.5.0: Discussion

To address the basic neural mechanisms of cortical electrotherapy, in the present report we used *in vitro* whole-cell recordings and uniform electric field stimulation. A necessary step toward the rational design of sub- and suprathreshold brain stimulation paradigms is a systematic and quantitative method for predicting which neuronal elements respond to electric fields; this analysis can then be scaffolded onto theories of network processing and the ultimate therapeutic outcomes.

3.5.1: Relevance of in vitro data to clinical brain stimulation

Several factors concomitantly facilitate the precise characterization of electric field effects *in vitro*, while qualifying how *in vitro* data is used to understand and design clinical electrotherapies. The application of uniform electric fields to brain slice preparations (Jefferys, 1981; Chan and Nicholson, 1986; Gluckman et al., 1996; Svirskis et al., 1997; Francis et al., 2003; e.g. Bikson et al., 2004; Deans et al., 2007; Radman et al., 2007) results in each cell exposed to an identical 'electrical environment', such that differences in neuronal responses can be attributed (and correlated) directly to differences in neuronal morphological/biophysical characteristics (Fig. 3.1). Only in cases where electric fields induced in the brain for clinical therapies and research are uniform on the scale of a single neuron, as may be the case for non-invasive stimulation or distant cortical electrodes, can our data be used to directly predict neuronal response to the specific 'quasi-uniform' electric field at each location (e.g. cortical area) in the brain.

In brain slices, the majority of afferents are cut, and intact synapses are inactive compared to the *in vivo* situation (McCormick et al., 1985; Meyer, 1987). These changes affect cellular properties such as resting membrane potential and conductance, as well as AP threshold. Similarly, spontaneous network oscillations, and other forms of 'tonic' system drive, which may modulate neuronal sub- and suprathreshold response (Parra and Bikson, 2004; Lakatos et al., 2005), are absent in brain slices superfused with "normal" ACSF.

In response to *subthreshold* stimulation, in the absence of (by definition) electric-field induced synaptic activation, and ongoing neuronal oscillations (*in vitro*), *neuronal morphology* merits investigation as a predictor of neuronal response. Our morphological reconstructions account for, in part, the inherent cutting of some dendritic processes during brain slice preparation.

Suprathreshold responses integrate the direct neuronal response to the electric field and the cumulative synaptic response by the network. Thus *cell type*, encompassing laminar position, network connectivity, and neuronal morphology merits investigation.

3.5.2: Response to subthreshold fields

It is well established, that in response to subthreshold electric fields, neurons polarize in a compartment specific fashion with compartments oriented towards the anode generally hyperpolarizing and compartments oriented towards the cathode depolarizing (Jefferys, 1981; Chan and Nicholson, 1986; Maccabee et al., 1993; Delgado-Lezama et al., 1999; Francis et al., 2003; Bikson et al., 2004). Somatic polarization may be reflected as a corresponding change in spontaneous firing rate (Terzuolo and Bullock, 1956; Hern et al., 1962; Purpura and McMurtry,

1965). Neuronal cell types with a non-symmetric dendritic morphology are preferentially modulated by the electric field (Hern et al., 1962; Chan et al., 1988).

Our results indicate that based only on volume-weighted neuronal morphology (without considering cell/compartment specific membrane biophysics) the polarity of cortical neuron somatic membrane polarization by uniform fields can be predicted with high fidelity, and the magnitude of polarization approximated, using the volume-weighted polar histogram coherence vector (described by the mean angle and vector length).

The polar histogram coherence vectors provide a parsimonious model of cortical neuron morphology in relation to electric field induced somatic polarization. Its intuitive applicability, independence of non-linear cellular biophysics, and lower computational overhead gives it merit. This intuitive approach is thus applicable to predict subthreshold polarization from solely morphological data. For example, because the vector length is lower for symmetric cells, (e.g. some interneurons; Fig. 3.6), the polar histogram model predicts reduced maximum somatic polarization length (λ_p) for such cells compared to larger, more asymmetric (e.g. pyramidal) cells with a higher vector length. The model also predicts that optimal positive and negative polarization length, for any given cell, is achieved for mean angles of 90° and 270° respectively, aligned with the electric fields. Cells with mean angles perpendicular to the direction of the electric field (0° or 180°) are predicted not to polarize significantly (low λ_p), regardless of vector length.

However, the polar histogram coherence vector model neglects weighting of neuronal segments by their proximity to the soma and distributed cellular biophysics. Indeed, though the dependence of the observed polarization on polar histogram morphological variables is

significant ($p < .001$) this parsimonious model does not account for almost half of the observed variance ($r^2 = .41$). Given compartment specific biophysical parameters for each neuron, the 2nd derivative of the extracellular voltage along the membrane (i.e. activating function; McIntyre, 1999; McIntyre, 2000) would yield more accurate predications (morphological data shall be published on www.neuromorpho.org).

Individually, Layer V pyramids exhibited the highest measured somatic sensitivities to subthreshold fields (polarization lengths, λ_p), and the highest polar histogram vector lengths, a measure of the asymmetry of the volume of neuronal membrane in relation to the soma. Applied *subthreshold* electric field therapies (tDCS, tACS), if quasi-uniform across cortical regions, would thus preferentially polarize Layer V cell somas. Human cortical neurons can be longer than the rat cortical neurons investigated here (Meyer, 1987). However, assuming the ratio of volume between the sum of apical and basal neuronal elements is similar between rat and human cortical neurons, then despite differences in overall size the polar histogram metric would scale accordingly to predict a similar distribution of *somatic* polarization differences across species (Fig. 3.3).

Distal terminal electric field induced polarization is important to quantify because: a) the maximum polarization is thought to occur at the terminals (Tranchina and Nicholson, 1986; Chan et al., 1988; Maccabee et al., 1993), and b) dendrite polarization will modulate neuronal processing (e.g. the site of synaptic input (Bikson et al., 2004). The distal polarization of a symmetrically branching dendritic tree has been modeled (Tranchina and Nicholson, 1986), in one case with approximately 2.5 times greater polarization at the distal terminal than at the soma (Hause, 1975). We emphasize that basal and apical dendrites will concomitantly polarize in

opposite directions, thus it is incorrect to describe any electric field (experimentally or clinically) as globally de- or hyperpolarizing.

3.5.3: Response to suprathreshold fields, mechanisms of AP initiation

Several lines of evidence suggest that AP initiation in response to uniform electric fields cannot be explained by a simple linear depolarization of the soma to threshold: (1) While the values of subthreshold polarization per unit electric field recorded at the soma linearly correlated to field polarity, in some cells, spiking was initiated with fields of either polarity, or of polarity opposite to the sub-threshold polarization value; (2) The values of subthreshold polarization per unit electric field recorded at the soma, multiplied by the electric field induced firing threshold (expected somatic polarization at threshold electric field) is less than the difference between resting membrane potential and action potential threshold (expected somatic polarization necessary for somatic AP initiation); an extreme example was a cell with a sub-threshold somatic polarization value of 0 $mV*(mV/mm)^{-1}$ and electric field firing threshold of 72 mV/mm; (3) EPSPs were evident in most cells recorded during stimulation, and were dependent on glutamatergic synaptic activity; (4) The DC chronaxie values for electric field stimulation were lower than for intracellular current injection reflecting differing neuronal elements triggering AP initiation for the two stimulation cases (Nowak and Bullier, 1998), and/or synaptic contributions towards electric field induced firing threshold. The spatial profile of stimulation may also impact chronaxie measurements; with neuronal elements charging and summing in parallel during uniform electric field stimulation. Related to this latter point, (5) some cells that were not

categorized as "intrinsically bursting" in response to intracellular current injection (see Methods), exhibited bursting behavior when stimulated by electric fields.

Bursting has been hypothesized as dependent on the opening of hyperpolarization-activated channels of a distal dendritic region (e.g. by inhibitory inputs), while an action potential generated in a depolarized region of the cell back-propagates to this distal hyperpolarized region resulting in dendritic calcium spikes (Lu et al., 1992; Lesica and Stanley, 2004; Izhikevich, 2005). The original action potential and subsequent dendritic spikes may be observed from a somatic recording as a burst response. In contrast to intracellular current injection, electric fields simultaneously de- and hyperpolarize distinct neuronal compartments (Figure 2.1), This may be a mechanism for the observed modulation to bursting in response to the electric field.. We have observed modulation of firing to a burst response in pyramidal cells, where distal and basal compartments are electrotonically distant (Larkman et al., 1992).

3.5.4: Response to suprathreshold fields

In coronal *in vitro* brain slices, individual Layer V/VI cells demonstrated the lowest AP thresholds in response to 100 ms uniform electric fields. We have found evidence for both direct and orthodromic activation of layer V/VI cells. However, it is important to emphasize that recruitment order is a spectrum across cell types, consistent with a network/orthodromic contribution to activation for most cells. One goal of probing cortical slices with suprathreshold electric fields is to characterize the utility of cortical brain slices as a research tool for suprathreshold non-invasive transcranial stimulation (e.g. TMS). We have recorded a sparse sample of cortical neurons, with 3 of 34 cells exhibiting direct activation (without EPSPs) in

response to 100 ms pulses, and an unrelated minority of cells responded to short, TMS-like pulses. Lower stimulator outputs of laterial medial (l-m) TMS coil orientations or any stimulator outputs of posterior-anterior (p-a) TMS are considered only to induce (indirect) i-waves, while greater stimulator output in the l-m orientation is necessary to induce (direct) d-waves (Patton and Amassian, 1954; Brocke et al., 2005).

Despite experimental differences between *in vitro* uniform electric fields and human cranial stimulation approached, biophysical features governing suprathreshold response (e.g. morphology, cell type, connectivity) should be generalizable. *In vitro*, because all neurons were exposed to a uniform electric field, we demonstrated that differences in suprathreshold response can be attributed to (the uncontrolled variable of) biophysical distinctions of cortical cell types.

In addition, the absolute firing thresholds and recruitment order *in vitro* may be different than during clinical stimulation because of: 1) greater electric field non-uniformities during clinical stimulation, particularly the action potential initiation zones; 2) using *in vitro* preparations, portions of axons are inevitably cut, including corticospinal axons,that have been attributed to d-waves (Pascual-Leone et al., 1994; Rothwell et al., 1994) and corticocortical afferents linked to the generation of i-waves (Patton and Amassian, 1954; Nakamura et al., 1997); 3) the square pulse used here leading to differing neuronal activation than the mono- or biphasic waveforms generated by TMS (Sommer et al., 2002), while the pulse lengths used in TMS and TES are much shorter as well; 4) differences in size, length constant, and morphology between human and rat cortical neurons; 5) ongoing network activity (e.g. state dependant activation).

For the reasons noted above, *in vitro*, only a minority of neurons fired in response to 500 μs electric field step pulses with amplitudes up to the maximum possible for our experimental setup, which encompasses the reported range of clinical TMS motor-evoked potential (MEP) threshold amplitudes of 30 to 130 mV/mm (Epstein et al., 1990; Rudiak and Marg, 1994; Thielscher and Kammer, 2002). In addition, the observed recruitment orders across cortical cell types in response to 100 ms square pulses, may not hold for sub-500 μs pulses probed at even higher intensities than used here, possibly because at this timescale summation of direct electric field polarization and (delayed) EPSP induced polarization is not possible. Additionally, the capacitance of differing cortical cell types/cellular compartments may change polarization induced by electric fields of varying pulse lengths (Tehovnik et al., 2006; Peterchev et al., 2008).

3.5.6: Towards a mechanistic understanding and rational design of clinical cortical brain stimulation

Which neuronal elements are activated by electrical stimulation are considered to underlie the ultimate behavioral and therapeutic outcomes (Ranck, 1975). Central to this idea is that not all neurons will be equally effected by a given stimulation protocol, and that distinct stimulation protocols target distinct neuronal populations/neuronal compartments. Therefore, determining *which cells are acutely modulated by stimulation is a pivotal first step toward the rational design of electrotherapies*: however, this is only a first step toward the complex analysis of how electrical stimulation affects information processing, synaptic plasticity, network function and ultimately behavior. Conversely, network activity may affect both subthreshold polarization sensitivity (polarization length, λ_p) and suprathreshold recruitment order. The present study

addressed only the first step by taking advantage of the isolated brain slice preparation.

Development of subthreshold stimulation paradigms should consider the polarization of specific neuronal compartments (such as the soma or specific dendritic terminals), in the context of their roles in ongoing neuronal processing. For the range of electric fields induced by typical subthreshold clinical electrotherapies (e.g. tDCS), the predicted membrane polarization is on the order of mV; even at the tufts of the largest cortical neurons (Hause, 1975). How can such relatively small polarizations lead to significant functional changes in the brain? When considered in the context of ongoing activity, we have shown that acutely, weak fields may be amplified at the single cell (Radman et al., 2007) and network (Parra and Bikson, 2004) levels, through changes in spike timing. In addition to these acute "amplification" mechanisms, it is necessary to characterize the plastic effects of electrical stimulation protocols; for example *prolonged* weak depolarization (>10 minutes), is thought to lead to plastic changes as observed during tDCS (Nitsche and Paulus, 2000; Nitsche et al., 2003b; Nitsche et al., 2003a)..

The ultimate goal of rational electrotherapy is to promote changes in network function that alleviate behavioral symptoms while minimizing disruption of cognitive function. The characterization of cellular responses to stimulation is a necessary but incremental step toward this goal. In summary, the present study addresses the importance of cortical neuronal morphology and cortical cell type during sub- and suprathreshold electric field stimulation. These data are a necessary step toward a mechanistic understanding of clinical cortical electrotherapy, and the design of more targeted (e.g. focal, fewer side-effects, longer lasting) brain stimulation strategies.

Chapter 4

Appendix 1: One-dimensional representation of a neuron in a uniform electric field

4.1.0 Abstract

The neocortex is the most common target of sub-dural electrotherapy and non-invasive brain stimulation modalities including transcranial magnetic stimulation (TMS) and transcranial current simulation (TCS). Specific neuronal elements targeted by cortical stimulation are considered to underlie therapeutic effects, but the exact cell-type(s) affected by these methods remains poorly understood. We determined if neuronal morphology predicted responses to subthreshold uniform electric fields. We characterized the effects of subthreshold electrical stimulation on identified cortical neurons *in vitro*. Uniform electric fields were applied to rat motor cortex brain slices, while recording from interneurons and pyramidal cells across cortical layers, using whole cell patch clamp. Neuron morphology was reconstructed following intracellular dialysis of biocytin. Based solely on volume-weighted morphology, we developed a simplified model of neuronal polarization by sub-threshold electric field: an electrotonically linear cylinder that further predicts polarization at distal dendritic tree terminations. We found that neuronal morphology correlated with somatic sub-threshold polarization. Layer 5/6 pyramidal neuron somata (individually) and dendrites (averaging across neurons) were most sensitive to sub-threshold fields. This analysis was extended to predict a terminal polarization of a human cortical neuron as 1.44 mV per mV/mm electric field.

4.2.0: BACKGROUND AND SIGNIFICANCE

Fundamental questions remain regarding the cellular targets of transcranial direct current stimulation (tDCS), including the relative activation of morphologically and functionally diverse

groups of inhibitory interneurons and excitatory pyramidal cells. Neuronal segments closest to the stimulating anode (virtual anode for TMS) have been shown to hyperpolarize, and concomitantly the segments closest to the (virtual) cathode depolarize (Chan et al., 1988). In response to the unique electric fields induced by tDCS (Wagner et al., 2007b), neuronal membranes are considered to polarize in a "compartment" specific manner; the polarized compartments interact according to the electrotonic decay along the neuron (Rall, 1977; Larkman et al., 1992). Neuronal modeling (Hause, 1975; Tranchina and Nicholson, 1986; Rattay, 1989; Nagarajan et al., 1993) and *in vitro* (Bikson et al., 2004) studies of electric field stimulation have identified morphological features which govern the polarization of (interacting) neuronal compartments, including branching patterns and membrane space constants,. Changes of compartment angle relative to an applied electric field (e.g. activating function), branch terminations, or changes in inter-compartment impedance can determine the locations of entry and exit of induced transmembrane currents that lead to polarization (Tranchina and Nicholson, 1986; Rattay, 1989). The neuronal space constants (λ), and related diameter of axons and dendrites, govern the axial distribution of these induced transmembrane polarizations, and therefore regulate the degree to which neuronal compartments interact (Tranchina and Nicholson, 1986; Plonsey and Barr, 1998). Concurrent polarization of individual segments of a neuronal tree can lead to complex changes in overall neuronal function by modulating cellular biophysics (Valero-Cabre et al., 2005) including non-linear voltage-gated conductances, synaptic efficacy, and AP threshold or timing (Chan et al., 1988).

The goal of the present study was to determine if the distinct morphological features of cortical cell types affect their response to stimulation by electric field.

4.3.0: METHODS

Coronal slices (300 μm) of primary motor cortex (M1) were prepared from male P21-25 Sprague-Dawley rats as previously described (Ramos et al., 2008a; Radman et al., 2009 (in press)). Conventional whole-cell patch clamp recording techniques were used to measure activity from neurons in M1. Uniform electric fields were generated across individual slices by passing current between two parallel Ag/AgCl electrodes (Radman et al., 2007) placed on the bottom of a customized submerged chamber. The convention of electric field polarity used in the present report refers to the anode on the pial side of the cortex. The somatic steady-state transmembrane voltage response to ~ 5 mV/mm electric field steps, up to ~ +/-30 mV/mm, were linearly fit (Fig. 4.1), the slope of which was used as the subthreshold polarization per unit electric field applied, which is described in mV of polarization per mV/mm of electric field. Post-recordings, biotin-avidin-HRP histochemistry was performed as previously described (Ramos et al., 2008b). The tracing was aligned so the direction of the electric field traversed along the 90° line from the top of the tracing to the bottom. NeuroExplorer (Microbrightfield, Williston, VT, USA) branched structure analyses were used to determine segment angle (φ_{seg}), length (l_{seg}), diameter (d_{seg}), and volume information for each segment of each individual neuron's tracing.

For each cortical neuron, an electrotonically 1-dimensional cylinder was created integrating all segments of a neuronal tree, based on the diameter of each segment and its angle relative to the uniform electric field. We assumed a linear and symmetric distribution of electric field-induced polarization, maximal and of opposite polarity at each cylinder terminal (e.g. the dendrite tufts). The cylinder was divided into "apical" (towards the anode) and "basal" (towards the cathode)

sub-cylinders, anchored around the soma, such that the polarization of the soma was predicted by the relative sub-cylinder lengths (Figure 3.1A, B).

The effect of the uniform electric field to each segment was weighted by the sine of the segment angle (φ_{seg}) relative to the electric field, multiplied by that segment's length (l_{seg}) (Equation 1).

$$l_{proj} = \sin(\varphi_{seg}) \times l_{seg} \qquad \text{(Eq. 1)}$$

The resulting projected length along the direction of the field (l_{proj}) , was further adjusted to replace the original diameter (d_{seg}) with the largest diameter segment in the neuronal tree (d_{max}), but maintaining the same volume of the original segment, using the assumption of cylindrical segments (Equation 2).

$$l_{eq} = l_{proj} \times \frac{(d_{seg})^2}{(d_{\max})^2} \qquad \text{(Eq. 2)}$$

All apical and basal segments ($_{\cdot a}$, $_{\cdot b}$) were weighted and summed to give two respective combined cylinders (L_{apical} , L_{basal}):

$$L_{apical} = \sum_{\text{apical segment } a=1}^{i} l_{eq \cdot a} = \sum_{\text{apical segment } a=1}^{i} \sin(\varphi_{seg \cdot a}) \times l_{seg \cdot a} \times \frac{(d_{seg \cdot a})^2}{(d_{\max})^2} \qquad \text{(Eq. 3)}$$

$$L_{basal} = \sum_{\text{basal segment } b=1}^{i} - l_{eq \cdot b} = \sum_{\text{basal segment } b=1}^{i} \sin(\varphi_{seg \cdot b}) \times l_{seg \cdot b} \times \frac{(d_{seg \cdot b})^2}{(d_{\max})^2} \qquad \text{(Eq. 4)}$$

Finally, we assumed an induced polarization, varying linearly along the cylinder from $-E(\sqrt{d_{\max}}\, m)$ at the apical cylinder (anode proximal) terminal to $+E(\sqrt{d_{\max}}\, m)$ at the basal (cathodal proximal) terminal. The ratio of the difference of the apical and basal cylinders (L_{apical}, L_{basal}) to their sum represents the location of the soma, such that the voltage of the soma may be simply predicted as:

$$V_{soma} = E \times (m \times \sqrt{d_{\max}}) \times \frac{L_{apical} - L_{basal}}{L_{apical} + L_{basal}} \qquad \text{(Eq. 5)}$$

This holistic model is analogous to 1-dimensional cable theory predicting a peak terminal polarization, of a homogeneous equivalent cylinder with infinite-resistance terminals in a uniform field, of +/- $E\lambda$ mV for cylinders of length $L >> \lambda$ (Tranchina and Nicholson, 1986; Chan et al., 1988; Plonsey and Altman, 1988). λ is the cylinder's length constant equal to $\sqrt{d_{\max}} \times \sqrt{R_m} \div \sqrt{4R_i}$ (Rall, 1977; Larkman et al., 1992), L is the total equivalent cylinder length, R_m is the membrane resistivity, and R_i is intracellular resistivity. We incorporated an experimentally derived variable m, determined from fitting Eq. 5 to all morphologically reconstructed neurons; m approximates the relations of the membrane (R_m) and axial (R_i) resistivity in the equation for space constant (λ): , $\sqrt{d_{\max}} \times \sqrt{R_m} \div \sqrt{4R_i}$, thus $\lambda \approx \sqrt{d_{\max}} \times m$. We then used this value of m to estimate the theoretical distal terminal polarization of $E\lambda$ as $E(\sqrt{d_{\max}}\, m)$.

4.4.0: RESULTS

4.4.1: Neuronal morphology, relative to applied electric field, correlates induced subthreshold polarization: one-dimensional transformation of neuronal morphology and predictions of distal terminal polarization.

A total of 51 neurons from M1 were recorded, 36 of which were identified by cortical layer and cell type. The direction of cortical sub-threshold somatic polarization increased linearly with increasing electric field steps, and reversed polarity with the direction of the applied electric field

One dimensional electrotonic approximations of neuronal branching have previously been proposed for simplified structures (Tranchina and Nicholson, 1986; Larkman et al., 1992). We developed an automated transformation, for any morphologically reconstructed neurons, into an electrotonically 1-dimensional cylinder with a linear distribution of polarization; the polarization varying from $-Em\sqrt{d_{\max}}$ at the distal apical (closest to the anode) terminal, to $+Em\sqrt{d_{\max}}$ at the distal basal (closest to the cathode) terminal. For each neuron, all segment volumes were weighted according to the segment's angle to the electric field, and all apical and basal segments where then combined into respective cylinders with diameter equal to the maximal diameter (d_{max}) of the original neuronal tree (see Methods). The position of the soma was determined at the junction of apical and basal cylinders, such that somatic polarization may be predicted (Fig. 4.1A and B, and methods equations 1-5). The cylinder's space constant, λ, was estimated as the square root of the diameter of the cylinder, , d_{max}, scaled by a variable, m. The scaling variable m is common across all neurons, and derived from the best fit of the electrotonically 1-dimensional predictions of somatic polarizations, to experimentally recorded values (variable m=.21, $p < .05$, $r^2 = .55$, n=30, Fig. 4.1C).

Analytical models predict a maximal polarization of +/- $E\lambda$ at the distal terminals of an homogenous cylinder in a uniform electric field , when $L >> \lambda$; where L is the total equivalent cylinder length (Tranchina and Nicholson, 1986; Plonsey and Altman, 1988). Approximating λ using $m\sqrt{d_{\max}}$ (see methods), we predicted distal terminal subthreshold polarization sensitivities

of $E\ m\sqrt{d_{\max}}$. A significant difference was found between predicted distal subthreshold polarization ($m\sqrt{d_{\max}}$) of interneurons across layer, compared to either L2/3 ($p < .03$) or L5/6 ($p < .02$) pyramids (T-test, Fig. 4.1D).

Fig. 4.1 (below). Electrotonically linear 1-D model: Neuronal morphology predicts somatic and dendritic tuft sensitivity to sub-threshold electric fields. ***A,*** **Example morphological reconstruction of a L5 regular spiking pyramidal neuron with electric field induced somatic polarization of 0.14 mV*(mV/mm)$^{-1}$. The left circle indicates the largest segment diameter for this neuron's segments, d_{max}. The right circle and inset illustrates a sample segment length, *l*; segment diameter, *d*; and angle with respect to the electric field, φ; used to construct the 1-D cylinder in *B*.** ***B,*** **1-D cylinder model of transmembrane polarization. Schematic (left) represents construction of equivalent neuron with apical and basal combined cylinders and soma. Linear distribution of polarization along the equivalent neuron is plotted (right), with maximal polarization of +/- $Em\sqrt{d_{max}}$ at the distal ends of the neuron. Equations represent construction of apical and basal cylinders, using variables illustrated in *A*.** ***C*****, For all reconstructed neurons, the 1-d model of *B* is applied to predict somatic polarization (x-axis), and correlated to experimentally recorded somatic transmembrane polarization ($p < .05$, $r^2 = .55$, n=30).** ***D,*** **The slope, *m*, of the best fit line in *C* is then used as a general membrane property constant (see Methods) that is multiplied by each individual neuron's $\sqrt{d_{max}}$ to predict terminal polarization. 1-D cylinder model predictions of terminal polarization, separated according to cortical cell type, yields a statistically significant difference between interneurons and L5/6 pyramidal neurons ($p < .02$) as well as between interneurons and L2/3 pyramidal neurons ($p < .03$).**

1

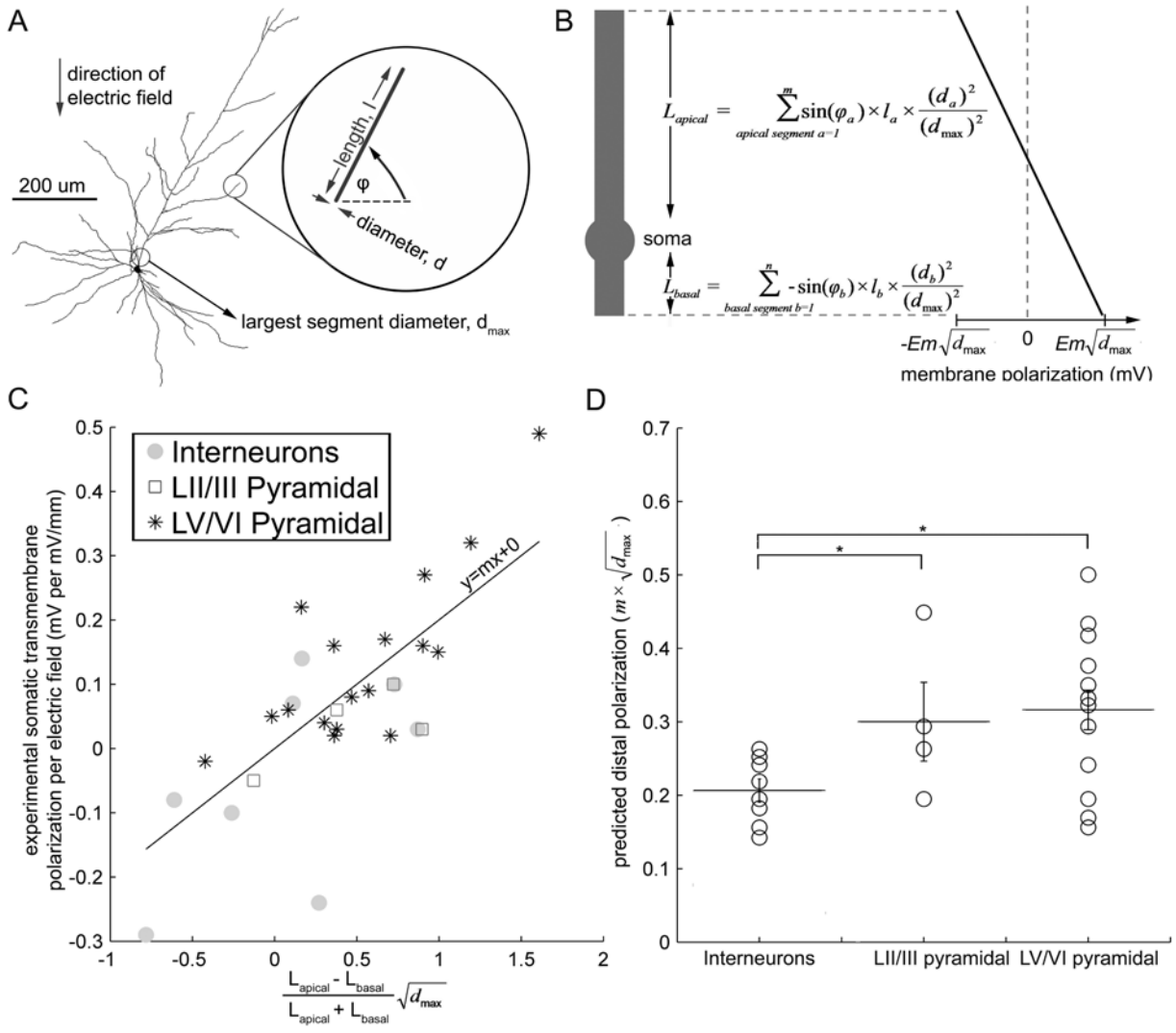

4.5.0: DISCUSSION

4.5.1: Response to subthreshold fields, implication to tDCS

Our results indicate that based only on volume-weighted neuronal morphology (without considering cell/compartment specific membrane biophysics) the polarity of cortical neuron somatic membrane polarization by uniform fields can be predicted with high fidelity, and the magnitude of polarization approximated, using the 1-dimensional cylinder transformation of neuronal morphology.

Human cortical neurons can be longer, with a larger maximal segment diameter, than the rat cortical neurons investigated here (Meyer, 1987). Assuming the ratio between the sum of apical and basal neuronal elements is similar, between rat and human cortical neurons, despite differences in overall size, our metrics predict a similar distribution of *somatic* polarization differences across species (Figure 2). If we consider a maximal segment diameter of an illustrative human layer 5 neuron to be 10 μm (Meyer, 1987), the electrotonically 1-D model of terminal polarization, $Em\sqrt{d_{\max}}$, predicts a terminal polarization sensitivity of ~ .66 mV per mV/mm of electric field induced. This value is moderately higher than the maximal predicted terminal polarization predicted for rat cortical neurons (up to .5 mV*(mV/mm)$^{-1}$). Note we are making the assumption that the experimentally derived variable *m*, dependent on the cell specific axial and membrane resistance, is the same across these species. During conventional tDCS, peak cortical fields may be of magnitudes from .43 to 1.09 mV/mm per 1 mA of total surface electrode current (Datta et al., 2008) across human cortex, resulting in a predicted terminal polarization of ~ .28 to .72 mV per 1 mA. Up to 2mA are commonly used in tDCS experiments, thus the peak terminal polarization prediction is 1.44 mV. Small changes in membrane polarization may be amplified through non-linear neuronal processes. Previous models (Hause, 1975) show somatic polarization of .17 mV per 1 mV/mm electric field applied. Their maximum terminal polarization is .46 mV per mV/mm electric field. In summary, these results demonstrate the importance of cortical neuronal morphology and cortical cell type during sub- and suprathreshold electric field stimulation

Chapter 5

Appendix 2

5.1.0: *In vitro* modulation of endogenous rhythms by AC electric fields: Syncing with clinical brain stimulation

Humans are exposed to an increasing prevalence of weak and strong AC electric fields, as part of daily life in the modern world. Further, electric fields are being deployed to modulate brain function for research and clinical applications. A single electric field pulse, applied via transcranial electrical or magnetic stimulation, can transiently excite or disrupt activity in neural circuits. In contrast, extended exposure to steady electric fields or pulse trains can result in long-term effects on neural activity including potentiation or depression. In addition, it has been demonstrated that brain stimulation with electric fields can improve cognitive performance in normal subjects (Marshall et al, 2006). The impact of electric fields on brain function has motivated the development of therapies to treat a wide range of psychiatric and neurological diseases using transcranial electrical or magnetic stimulation (Wassermann & Lisanby 2001), as well as deep brain stimulation with implanted electrodes.

The mechanisms by which electric fields affect brain function have not been fully elaborated. A recent report in the Journal of Physiology by Deans et al (2008) presents new data on the interaction of AC electric fields down to a cellular level as well as with neuronal population dynamics. The report reveals a frequency-specific ability of AC electric fields to rhythmically polarize pyramidal neurons of the CA3 region of the hippocampus and demonstrates the ability of AC fields to alter pharmacologically induced endogenous oscillations in the hippocampus. These data have important implications for understanding the effect of

environmental AC fields and therapeutic stimulation on the activity of neuronal ensembles. A central finding of this study is that an AC electric field, applied *in vitro* to a brain slice set to oscillate in the gamma frequency range through bath application of kainate, shifts the ongoing oscillation to center on the applied field frequency or a subharmonic of that frequency. This review of Deans et al. is intended to elucidate the connection between their work and other recent *in vitro* findings concerning electric fields in the brain with some recent clinical findings pertaining to cognitive function and electric fields.

5.1.1 Sensitivity of CA3 pyramidal neurons to AC electric fields

An understanding of the frequency dependence of the passive membrane properties of individual CA3 pyramidal neurons to polarization by an electric field was pertinent towards subsequent characterization of the effects of AC electric fields on ongoing oscillations. Coupling of the electric field to the cell's transmembrane potential decreased exponentially with increasing stimulation frequencies, consistent with the commonly modeled resistor-capacitor circuit across the membrane. Sharp intracellular recording techniques were employed to record changes in transmembrane potential induced by the oscillating electric field applied across the transverse hippocampal slice. The results were reinforced with optical measurements, in order to ensure accurate passive electrical property measurements of the unperturbed cell membrane. At frequencies below 10 Hz, the electric field did not differ in its efficacy to polarize the neuron, while 50 Hz neared the minimum efficacy for the range of frequencies tested (up to 100 Hz), resulting in approximately one-third the polarization efficacy compared to DC electric field polarization. This relationship of polarization by an electric field at differing frequencies

provides important information for the design of brain stimulation protocols, necessary when determining electric field strength at varying frequencies. For example, the response threshold in many TMS experiments is determined by single-pulse titration, whereas subsequent stimulation, with intensity normalized to this threshold, is at a higher frequency which could alter the effective threshold. In addition, the polarization enduced at 50Hz, Europe's power line frequency, and a similar effect at the United States' 60 Hz power-line frequency (see Deans' supplementary material), reveals the minimum electric field magnitude shown to have an effect is well below the magnitude of environmental fields caused by power-lines.

5.1.2 AC electric field modulation of kainate-induced gamma band oscillations

Upon deducing the efficacy of AC fields on polarization, the ability of these fields to modulate ongoing kainate-induced gamma band (~ 30 Hz) oscillations was demonstrated. Deans et al. show a 50 Hz AC electric field reducing the power at the ongoing oscillation frequency of 30 Hz, while shifting and increasing the power maximum slightly below this frequency to 25 Hz. Negative extracellular spikes in the ongoing gamma oscillation were shown to occur every other cycle of the 50 Hz AC field minima. On the other hand, when the control oscillation had a peak power of < 25 Hz (beta band) the field-induced modulation centered on 17 Hz or every third cycle. This effect of entrainment of the ongoing oscillation at the closest dividend of the field frequency may prove to have important clinical applications. Clinical studies have used a matching slow wave frequency field to provide entrainment of slow waves, though other frequencies may also prove effective for both slow wave and other oscillation band entrainment. This finding may allow clinical application of multiple band modulation such as theta modulated

gamma or sleep spindles (12-20 Hz) with slow-wave sleep (i.e., matching one frequency band while maintaining a dividend of another).

Deans et al. show maximal firing preceding peak soma depolarization by 5 ms. Concomitantly with this study, it has been shown that AC electric fields can constrain the firing of a single CA1 pyramidal cell to the rising edge of the depolarization, with the degree of coherence governed by the ratio of extracelullar field oscillation to intracellular drive towards firing threshold (Radman et al., 2007). Likewise, firing on the rising edge of an applied Gaussian waveform electric field occurred in either the positive or negative polarity (Francis et al., 2003). Francis et al. applied AC fields in the form of a series of positive or negative Gaussian pulses allowing entrainment of an elevated potassium-induced oscillation. They showed a dose dependent response at this lower frequency field and oscillation, as did Deans et al. Both research groups were unable to detect an effect below 0.3 mV/mm field strengths.

This work is particularly timely given increasing interest in the role of endogenous electric fields as neuronal signals, and clinical demonstration of applied weak current modulating memory and behavior (Marshall et al. 2006). Marshall et al. recently employed transcranial electrical stimulation to humans during slow wave sleep to improve performance in a word-recall task (declarative memory). It was presumed this effect was due to the electric field boosting slow wave oscillations which have previously been implicated in learning. This is an exciting finding, and Deans et al. have provided timely *in vitro* evidence for an underlying mechanism. In Marshall et al., the electric field frequency was selected to match the desired oscillation to be modulated—slow wave sleep (<1 Hz). In other studies, sleep slow waves were shown to be triggered with < 1 Hz transcranial magnetic stimulation pulses, though these pulses were of

suprathreshold magnitude, and possibly induced slow waves through a different mechanism. Deans et al. have now shown that at these frequencies there is no reduction in polarization efficacy by an electric field from the maximum possible for a neuron.

It is remarkable that a 0.5 mV/mm electric field at 50 Hz, resulting in a peak polarization of 25 μV intracellularly which is a small fraction of the difference between rest and firing threshold, has the ability to entrain an oscillating network. Deans et al. *in vitro* work is clearly important for clinical brain stimulation research. Corroborating and extending this study should provide enhanced understanding of the role of endogenous fields, as well as to greater specificity of electrical and magnetic stimulation, with fewer side effects. A key objective of future work should be the *in vitro* examination of the chronic effects of stimulation. Such research could reveal ways to optimize therapeutic efficacy, though the disconnected nature of *in vitro* slice networks may limit the applicability of these results to the intact brain.

5.2.0: A low-cost electrophysiology lab for high school students

5.2.1: Background and Significance

Electrophysiological recordings and signal analysis are a great passion for many neuroscientists (e.g. Buzsaki 2006). Unfortunately, the extreme cost of an electrophysiological recording system is poses a challenge for incorporation into undergraduate neuroscience laboratories. Education in the growing field of biomedical engineering is a necessity for expanding the employment options of students. The complexity of biomedical engineering creates challenges in creating exciting curriculum at the early stages of the undergraduate degree when students have limited laboratory skills. Efforts have been made towards reducing electrophysiology lab costs (Bruce et al. 2001). Here we present the results of our attempts to simplify these labs as much as possible. It is our hope that sacrificing some accuracy in recordings, for the sake of ease of use by students, will achieve our goals of a low cost electrophysiology lab able to be completed by undergraduates.

Neural recordings may be divided into three parts: signal transduction, amplification, and data acquisition. Here we have chosen the heart EKG signal for it's simple transduction into electrical energy via readily available Ag/AgCl surface electrodes. The amplification stage has been paired down to its simplest form, a single chip amplifier that is easily assembled by the students. The data acquisition stage employs previously develop free software that utilizes the readily available pc soundcard ("g-PRIME", Lott 2007).

5.2.2: Methods

Table 5.1: Equipment List

Description and Manufacturer Part Number (P/N)	Approximate Cost
Amplifier Integrated Circuit Chip #AD620BN-ND	$8.96
Twin Industries Breadboard #TW-E41-102B	$19.74
3M Breadboard Jumper Wire Kit 350PC, Digikey # #923351-ND	$32.14
EKG leads, Vermed #VMB20900-18-BLK	$3.15
EKG electrodes, Vermed #A10005-60	$2.12
2 Battery connectors, Digikey #BHV-W-ND	$1.72
2 9V Batteries	$3.00
Mono audio cable, Digikey #CP-2205-ND	$2.64

5.2.3: Constructing the circuit

Powerpoint slides for step by step construction of the circuit are available as supplementary material. The procedure is as follows:

1. Place the AD620 chip onto the breadboard, directly center between numbers 54 and 57 with notch facing the top of breadboard (the notch in the chip should face towards row 54).

2. Thread one end of a wire through the black binding post of the breadboard, labeled V_a, and the other end of that wire into one of the holes in row 56, to the left side of the chip. Row 56 should line up with pin three of the AD620 chip, this is the positive input pin (Figure 4.1). Also thread one of the EKG leads through the same binding post and screw down the binding post so the wires cannot fall out.

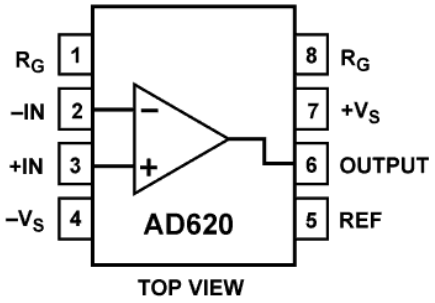

Figure 5.1: AD620 pin-out diagram

3. Thread one end of another wire through the red binding post of the breadboard, labeled V_b, and the other end of that wire into one of the holes in row 55, to the left side of the chip. Row 55 should line up with pin two of the AD620 chip, this is the negative input pin (Figure 4.1). Also thread one of the EKG leads through the same binding post and screw down the post.

4. Thread one end of another wire through the green binding post of the breadboard, labeled with the "ground" symbol, and the other end of that wire into one of the holes in row 57, to the right side of the chip. Row 57 should line up with pin five of the AD620 chip, this is the ground pin (Figure 4.1). Also thread one of the EKG leads through the same binding post, as well as the (thinner) black wire from the mono headphone jack connector, and screw down the post.

5. The negative battery rails will be along the left side of the breadboard. Run a wire from one of the holes above the "+" symbol on the leftmost side of the breadboard to the ground pin of the AD620, on row 57 on the right side of the chip (there should already be another wire in this

row). Also run a wire from one of the holes above the "-" symbol on the leftmost side of the breadboard to the negative power supply pin of the AD620, pin 4 of the chip (Figure 4.1), on row 57 on the right side of the chip.

6. The positive battery rails will be along the right side of the breadboard. Run a wire from one of the holes above the "-" symbol on the rightmost side of the breadboard to the ground pin of the AD620 (Figure 4.1), on row 57 on the right side of the chip (there should already be two other wires in this row). Also run a wire from one of the holes above the "+" symbol on the rightmost side of the breadboard to the positive power supply pin of the AD620 (Figure 4.1), pin 7 of the chip, on row 55 on the right side of the chip.

7. Connect the red wire from the mono audio connector the output pin of the AD620 (Figure 4.1), pin 6, on the right side of row 56. The other end of the mono audio connector is plugged into the audio input of your computer's soundcard.

9. Connect the 50 ohm resistor,

8. If the one chip amplifier circuit is to be constructed by the students, the power supply wiring should be double checked by the professor to ensure safe operation. Another option is for the professor to construct the amplifier or at least the power supply connections. The power supply wiring may also be glued in place so they are not moved between labs. To connect the negative power supply, connect the red lead from one of the battery connectors to one of the holes above the "-" symbol at the leftmost side of the breadboard. Connect the black lead from this battery connector to one of the holes above the "+" symbol at the leftmost side of the breadboard. To connect the positive power supply, connect the red lead from one of the battery connectors to one of the holes above the "+" symbol at the rightmost side of the breadboard. Connect the black

lead from this battery connector to one of the holes above the "-" symbol at the rightmost side of the breadboard.

Figure 5.2 illustrates a diagram of the completed breadboard.

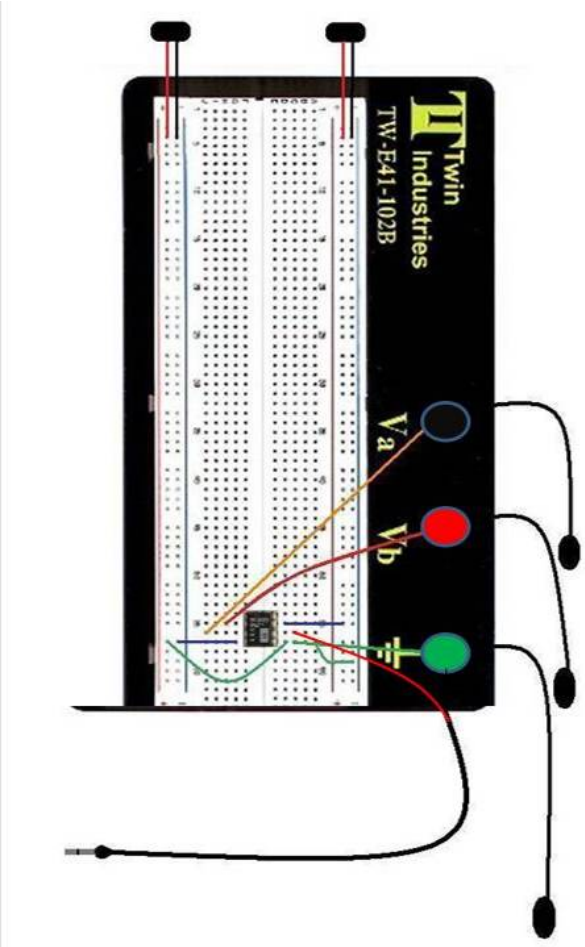

Figure 5.2: Low-cost EKG circuit breadboard

5.2.4: g-PRIME

g-PRIME is used here for data acquisition and analysis (Lott 2007). The free software is available for download at http://crawdad.cornell.edu/gprime/ . After installing and loading g-prime, choose your soundcard in the device menu. Add the active channel using the "Add Channel" button. The time axis of the oscilloscope plot is modified using the "Full Spans (s)"

drop-down menu. The voltage axis of the oscilloscope plot is modified using the "Volts per Division" drop-down menu.

5.2.5: Results

The results of a typical recording session results in robust QRS waves above the noise floor (Figure 4.3). The P and T waves may or not be discernible, depending on the noise environment the amplifier resides in.

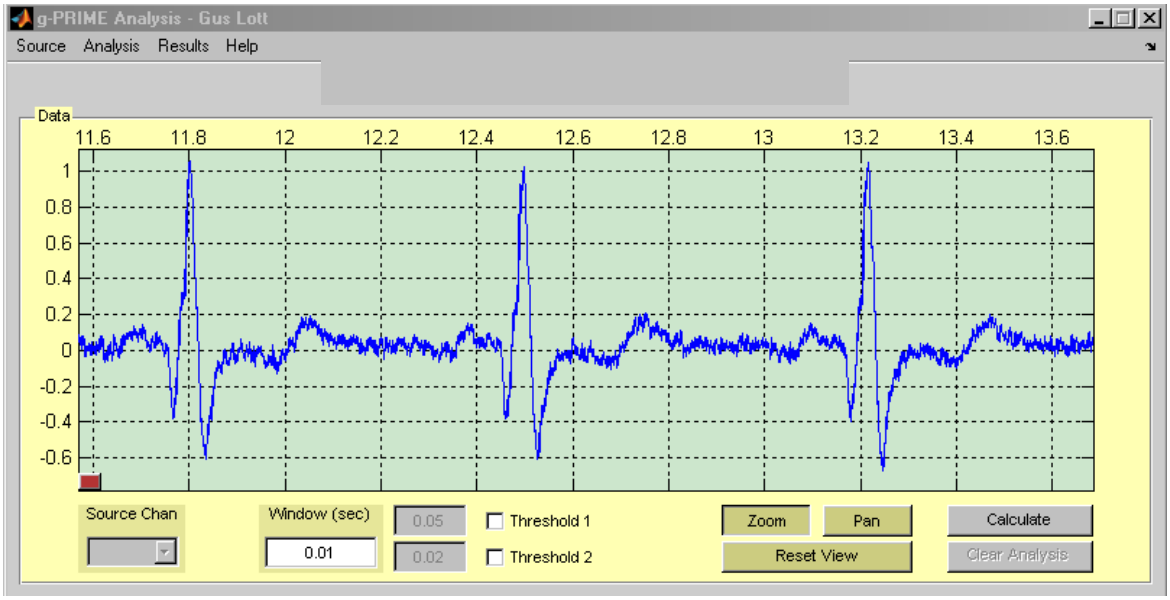

Figure 5.3: g-PRIME display with EKG waveforms recorded via low-cost circuit

5.2.6: Common Pitfalls

Noise from Laptop power supplies can sometimes create artifacts in the recordings. If this occurs, it may help to unplug the power supply *from the wall*.

Depending on your setups signal to noise ratio, a different sized resistor may be necessary. Smaller resistors create more gain (Eq. 1), and thus if the amplified signal is saturating the amplifier, using a larger resistor (and thus less amplification) may remedy this.

Many PCs have both “microphone” and “line-in” headphone input jacks. The microphone jack is designed for an unamplified microphone, and thus the jack amplifies the input signal internally. The dynamic range of a typical microphone port is only +/- 200 mV, whereas the rand of the line-in port is 2 V peak to peak (individual soundcards may vary, so check with your manufacturers). Exceeding this maximum voltage range may damage your soundcard.

Bibliography

Amassian VE, Eberle L, Maccabee PJ, Cracco RQ (1992) Modelling magnetic coil excitation of human cerebral cortex with a peripheral nerve immersed in a brain-shaped volume conductor: the significance of fiber bending in excitation. Electroencephalogr Clin Neurophysiol 85:291-301.

Amassian VE, Maccabee PJ, Cracco RQ, Cracco JB, Somasundaram M, Rothwell JC, Eberle L, Henry K, Rudell AP (1994) The polarity of the induced electric field influences magnetic coil inhibition of human visual cortex: implications for the site of excitation. Electroencephalogr Clin Neurophysiol 93:21-26.

Artola A, Brocher S, Singer W (1990) Different voltage-dependent thresholds for inducing long-term depression and long-term potentiation in slices of rat visual cortex. Nature 347:69-72.

Avery DH, Holtzheimer PE, 3rd, Fawaz W, Russo J, Neumaier J, Dunner DL, Haynor DR, Claypoole KH, Wajdik C, Roy-Byrne P (2006) A controlled study of repetitive transcranial magnetic stimulation in medication-resistant major depression. Biol Psychiatry 59:187-194.

Azouz R, Gray C.M. (2000) Dynamic spike threshold reveals a mechanism for synaptic coincidence detection in cortical neurons in vivo. PNAS 97(14):8110-8115

Badi AN, Hillman T, Shelton C, Normann RA (2002) A technique for implantation of a 3-dimensional penetrating electrode array in the modiolar nerve of cats and humans. Arch Otolaryngol Head Neck Surg 128:1019-1025.

Bikson M, Inoue M, Akiyama H, Deans JK, Fox JE, Miyakawa H, Jefferys JG (2004) Effects of uniform extracellular DC electric fields on excitability in rat hippocampal slices in vitro. J Physiol 557:175-190.

Bindman LJ, Murphy KP (1990) Delayed onset of potentiation in neocortical EPSPS during long-term potentiation (LTP)--a postsynaptic mechanism or heterogeneous synaptic inputs? Adv Exp Med Biol 268:307-312.

Bindman LJ, Lippold OC, Redfearn JW (1964) The Action of Brief Polarizing Currents on the Cerebral Cortex of the Rat (1) During Current Flow and (2) in the Production of Long-Lasting after-Effects. J Physiol 172:369-382.

Boggio PS, Ferrucci R, Rigonatti SP, Covre P, Nitsche M, Pascual-Leone A, Fregni F (2006) Effects of transcranial direct current stimulation on working memory in patients with Parkinson's disease. J Neurol Sci 249:31-38.

Bostock H (1983) The strength-duration relationship for excitation of myelinated nerve: computed dependence on membrane parameters. J Physiol 341:59-74.

Bragin A, Jando G, Nadasdy Z Hetke K Wise K Buzsaki G. (1995) Gamma (40-100 Hz) oscillation in the hippocampus of the behaving rat . J. Neurosc*i 15:47*

Bryant HL, Segundo JP (1976) Spike initiation by transmembrane current: a white-noise analysis. J Physiol`. 260(2):279-314.

Brocke J, Irlbacher K, Hauptmann B, Voss M, Brandt SA (2005) Transcranial magnetic and electrical stimulation compared: does TES activate intracortical neuronal circuits? Clin Neurophysiol 116:2748-2756.

Bruce R. Land, Robert A. Wyttenbach, Bruce R. Johnson, Tools for physiology labs: an inexpensive high-performance amplifier and electrode for extracellular recording, Journal of Neuroscience Methods, Volume 106, Issue 1, 30 March 2001, Pages 47-55

Brumberg JC, Nowak LG, McCormick DA (2000) Ionic mechanisms underlying repetitive high-frequency burst firing in supragranular cortical neurons. J Neurosci 20:4829-4843.

Brumberg JC, Hamzei-Sichani F, Yuste R (2003) Morphological and physiological characterization of layer VI corticofugal neurons of mouse primary visual cortex. J Neurophysiol 89:2854-2867.

Buzsaki G. Rhythms of the brain. New York: Oxford University Press; 2006.

Buzsaki G, Buhl DL, Harris KD, Csicsvari J, Czeh B, Morozov A. (2003) Hippocampal Network Patterns of Activity in the Mouse. Neuroscience 116:201

Canolty RT, Edwards E, Dalal SS Soltani M NAgajaran SS, Kirsch HE, Berger MS, Barbaro NM Knight RT (2006) High Gamma Power is Phase-Locked to theta OSciallations in Human Neocortex. Science 313:1625

Chan CY, Nicholson C (1986) Modulation by applied electric fields of Purkinje and stellate cell activity in the isolated turtle cerebellum. J Physiol 371:89-114.

Chrobak JJ, Buszaki G (1998) Gamma Oscillations in the Entorhinal Cortex of the Freely Behaving Rat. J. Neurosci 18:388

Chrobak JJ, Lorincz A, Buzsaki G (2000) Physiological patterns in the hippocampo-entorhinal cortex system. Hippocampus. 10(4):457-65.

Csicsvari J, Jamieson B, Wise KD, Buzsaki G. (2003) Mechanisms of gamma oscillations in the hippocampus of the behaving rat. Neuron. 37(2):311-22.

Chan CY, Hounsgaard J, Nicholson C (1988) Effects of electric fields on transmembrane potential and excitability of turtle cerebellar Purkinje cells in vitro. J Physiol 402:751-771.

Datta A, Elwassif M, Battaglia F, Bikson M (2008) Transcranial current stimulation focality using disc and ring electrode configurations: FEM analysis. J Neural Eng 5:163-174.

Deans JK, Powell AD, Jefferys JG (2007) Sensitivity of coherent oscillations in rat hippocampus to AC electric fields. J Physiol 583:555-565.

Deans JK, Bikson M, Fox JE & Jefferys JGR (2003). Effects of AC fields at powerline frequencies on gamma oscillations in vitro. Society for Neuroscience Annual Meeting 258.1

Delgado-Lezama R, Perrier JF, Hounsgaard J (1999) Local facilitation of plateau potentials in dendrites of turtle motoneurones by synaptic activation of metabotropic receptors. J Physiol 515 (Pt 1):203-207.

de Ruyter van Steveninck RR, Lewen GD, Strong SP, Koberle R, Bialek W (1997) Reproducibility and variability in neural spike trains. Science. 275 (5307): 1805-8.

DeWeese MR, Wehr M, Zador AM (2003) Binary spiking in auditory cortex. J Neurosci. 23(21):7940-9.

Donoghue JP, Sanes JN, Hatsopoulos NG, Gaál G (1998) Neural Discharge and Local Field Potential Oscillations in Primate Motor Cortex During Voluntary Movements. J. Neurophysiology 79, 159-173

Durand DM, Bikson M (2001). Suppression and control of epileptiform activity by electrical stimulation: a review. Proc IEEE 89, 1065–1082

Durand DM (2001) Suppression and control of epileptiform activity by electrical stimulation: a review. Proc IEEE 89:1065-1082.

Epstein CM, Schwartzberg DG, Davey KR, Sudderth DB (1990) Localizing the site of magnetic brain stimulation in humans. Neurology 40:666-670.

Esser SK, Hill SL, Tononi G (2005) Modeling the effects of transcranial magnetic stimulation on cortical circuits. J Neurophysiol 94:622-639.

Fischer Y, Wittner L, Freund TF, Gahwiler BH (2002) Simultaneous activation of gamma and theta network oscillations in rat hippocampal slice cultures. J Physiol. 539(Pt 3):857-68.

Faber DS, Korn H.(1983) Field effects trigger post-anodal rebound excitation in vertebrate CNS. Nature. 305(5937):802-4

Francis JT, Gluckman BJ, Schiff SJ (2003) Sensitivity of neurons to weak electric fields. J Neurosci 23:7255-7261.

Fregni F, Boggio PS, Nitsche M, Bermpohl F, Antal A, Feredoes E, Marcolin MA, Rigonatti SP, Silva MT, Paulus W, Pascual-Leone A (2005) Anodal transcranial direct current stimulation of prefrontal cortex enhances working memory. Exp Brain Res 166:23-30.

Fregni F, Boggio PS, Lima MC, Ferreira MJ, Wagner T, Rigonatti SP, Castro AW, Souza DR, Riberto M, Freedman SD, Nitsche MA, Pascual-Leone A (2006) A sham-controlled, phase II trial of transcranial direct current stimulation for the treatment of central pain in traumatic spinal cord injury. Pain 122:197-209.

Fricker D, Verheugen J, Miles R (1999). Cell-attached measurements of the firing threshold of rat hippocampal neurones. J Physiol 517.3, 791-804

Fujisawa S, Matsuki N, Ikegaya Y. (2004) Chronometric readout from a memory trace: gamma-frequency field stimulation recruits timed recurrent activity in the rat CA3 network. J. Physiol. 561(1): 123-131

Gatter KC, Sloper JJ, Powell TP (1978) The intrinsic connections of the cortex of area 4 of the monkey. Brain 101:513-541.

George MS, Lisanby SH, Sackeim HA (1999) Transcranial magnetic stimulation: applications in neuropsychiatry. Arch Gen Psychiatry 56:300-311.

Ghai RS, Bikson M, Durand DM (2000) Effects of applied electric fields on low-calcium epileptiform activity in the CA1 region of rat hippocampal slices. J Neurophysiol 84:274-280.

Gluckman BJ, Nguyen H, Weinstein SL, Schiff SJ (2001) Adaptive electric field control of epileptic seizures. J Neurosci 21:590-600.

Gluckman BJ, Neel EJ, Netoff TI, Ditto WL, Spano ML, Schiff SJ (1996) Electric field suppression of epileptiform activity in hippocampal slices. J Neurophysiol 76:4202-4205.

Hajos N, Palhalmi J, Mann EO, Nemeth B, Paulsen O, Freund TF (2004) Spike timing of distinct types of GABAergic interneuron during hippocampal gamma oscillations in vitro. J Neurosci. 24(41):9127-37.

Hamblin DL (2002) Effects of mobile phone emissions on human brain activity and sleep variables. International Journal of Radiation Biology 78(8):659-66Harris KD, Csicsvari J, Hirase H, Dragoi G, Buzsaki G (2003) Organization of cell assemblies in the hippocampus. Nature 424(6948):552-6.

Harris K, Henze D, Hirase H, Leinekugel X, Dragol G, Czurko A, Buzsaki G. (2002) Spike train dynamics predicts theta-related phase precession in hippocampal pyramidal cells. Nature 417:738-741

Hause L (1975) A mathematical model for transmembrane potentials secondary to extracellular fields. In: Electroanaesthesia: Biomedical and Biophysical Studies, A Edition (Sances J, Larson S, eds), pp 176–200. New York: Academic.

Heldman DA, Wang W, Chan SS, Moran DW (2006) Local field potential spectral tuning in motor cortex during reaching, IEEE Trans. Reh. Eng. 14(2)

Hern JEC, Landgren S, Phillips CG, Porter R (1962) Selective Excitation of Cortifgugal Neurones by Surface-Anodal Stimulation of the Baboon's Motor Cortex. J Physiol 161:73-90.

Izhikevich E (2005) Dynamical Systems in Neuroscience: Geometry of Excitability and Bursting: MIT Press.

Jefferys JG (1981) Influence of electric fields on the excitability of granule cells in guinea-pig hippocampal slices. J Physiol 319:143-152.

Jefferys JG, Deans J, Bikson M, Fox J. (2003) Effects of weak electric fields on the activity of neurons and neuronal networks. Radiat Prot Dosimetry.;106(4):321-3

Jones M, Wilson M. (2005) Theta rhythms coordinate hippocampal-prefrontal interactions in a spatial memory task. PLOS Biology 3(12): e402

Kahana M, Seelig J Madsen JR. (2001) Theta Returns. Curr. Opin. NeuroBiol. 11:739

Kara P, Reinagel P, Reid RC. (2000) Low response variability in simultaneously recorded retinal, thalamic, and cortical neurons. Neuron. (3):635-46.

Kashiwadani H, Sasaki YF, Uchida N, Mori K. (1999) Synchronized oscillatory discharges of mitral/tufted cells with different molecular receptive ranges in the rabbit olfactory bulb. J Neurophysiol. 82(4):1786-92.

Kincses TZ, Antal A, Nitsche MA, Bartfai O, Paulus W (2004) Facilitation of probabilistic classification learning by transcranial direct current stimulation of the prefrontal cortex in the human. Neuropsychologia 42:113-117.

Komssi S, Savolainen P, Heiskala J, Kahkonen S (2007) Excitation threshold of the motor cortex estimated with transcranial magnetic stimulation electroencephalography. Neuroreport 18:13-16.

Krings T, Buchbinder BR, Butler WE, Chiappa KH, Jiang HJ, Cosgrove GR, Rosen BR (1997) Functional magnetic resonance imaging and transcranial magnetic stimulation: complementary approaches in the evaluation of cortical motor function. Neurology 48:1406-1416.

Lakatos P, Shah AS, Knuth KH, Ulbert I, Karmos G, Schroeder CE (2005) An oscillatory hierarchy controlling neuronal excitability and stimulus processing in the auditory cortex. J Neurophysiol 94:1904-1911.

Larkman AU, Major G, Stratford KJ, Jack JJ (1992) Dendritic morphology of pyramidal neurones of the visual cortex of the rat. IV: Electrical geometry. J Comp Neurol 323:137-152.

Lesica NA, Stanley GB (2004) Encoding of natural scene movies by tonic and burst spikes in the lateral geniculate nucleus. J Neurosci 24:10731-10740.

Liebetanz D, Klinker F, Hering D, Koch R, Nitsche MA, Potschka H, Loscher W, Paulus W, Tergau F (2006) Anticonvulsant effects of transcranial direct-current stimulation (tDCS) in the rat cortical ramp model of focal epilepsy. Epilepsia 47:1216-1224.

Liu J, Newsome WT (2006) Local Field Potential in Cortical Area MT: Stimulus Tuning and Behavioral Correlations, J. Neuroscience, 26(30):7779-7790.

Lopez L, Chan CY, Okada YC, Nicholson C (1991) Multimodal characterization of population responses evoked by applied electric field in vitro: extracellular potential, magnetic evoked field, transmembrane potential, and current-source density analysis. J Neurosci 11:1998-2010.

Lott GK, "Hybridizing Cellular and Behavioral Neurobiology with Modern Engineering Tools: Microelectronics, Microfabricated Devices, and Software Solutions for Physiology," PhD Dissertation, Cornell University, 2007

Lu SM, Guido W, Sherman SM (1992) Effects of membrane voltage on receptive field properties of lateral geniculate neurons in the cat: contributions of the low-threshold Ca2+ conductance. J Neurophysiol 68:2185-2198.

Lutz A., Lachaux JP, Martinerie J, Varela F (2001) Guding the study of brain dynamics by using first person data: Synchrony patterns correlate with ongoing conscious states during a simple visual task. PNAS 99(3):1586-1591

Maccabee PJ, Amassian VE, Eberle LP, Cracco RQ (1993) Magnetic coil stimulation of straight and bent amphibian and mammalian peripheral nerve in vitro: locus of excitation. J Physiol 460:201-219.

Malinow, R., *Transmission between pairs of hippocampal slice neurons: quantal levels, oscillations, and LTP.* Science, 1991. **252**(5006): p. 722-724.

Mainen ZF, Sejnowski TJ (1996) Influence of dendritic structure on firing pattern in model neocortical neurons. Nature 382(6589):363.

Mainen ZF, Sejnowski TJ (1995) Reliability of spike timing in neocortical neurons. Science. 268(5216):1503-6.

Mann EO, Radcliffe CA, Paulsen O. (2005) Hippocampal gamma-frequency oscillations: from interneurones to pyramidal cells, and back. J Physiol. 562(Pt 1):55-63.

Marshall L, Helgadottir H, Molle M, Born J (2006) Boosting slow oscillations during sleep potentiates memory. Nature 444:610-613.

McBain C, Freund T, Mody I. (1999) Glutamatergic synapses onto hippocampal interneurons: precision timing without lasting plasticity. Trends in Neurosciences 22(5):228-235

McCormick DA, Connors BW, Lighthall JW, Prince DA (1985) Comparative electrophysiology of pyramidal and sparsely spiny stellate neurons of the neocortex. J Neurophysiol 54:782-806.

McIntyre CC, Grill WM (1999) Excitation of central nervous system neurons by nonuniform electric fields. Biophys J 76:878-888.

Mehta MR,Lee AK,Wilson MA. (2002) Role of experience and oscillations in transforming a rate code into a temporal code. Nature 417(6890):741-6

Meyer G (1987) Forms and spatial arrangement of neurons in the primary motor cortex of man. J Comp Neurol 262:402-428.

Miller R (1991) Cortico-hippocampal Interplay and the Representation of Contexts in the Brain. Springer-Verlag, New York

Miranda PC, Hallett M, Basser PJ (2003) The electric field induced in the brain by magnetic stimulation: a 3-D finite-element analysis of the effect of tissue heterogeneity and anisotropy. IEEE Trans Biomed Eng 50:1074-1085.

Miranda PC, Lomarev M, Hallett M (2006) Modeling the current distribution during transcranial direct current stimulation. Clin Neurophysiol 117:1623-1629.

Moore, D. S. and McCabe, G. P. (1999) Introduction to the Practice of Statistics, 3rd edition, New York: W. H. Freeman.

Nagarajan SS, Durand DM, Warman EN (1993) Effects of induced electric fields on finite neuronal structures: a simulation study. IEEE Trans Biomed Eng 40:1175-1188.

Nakamura H, Kitagawa H, Kawaguchi Y, Tsuji H (1997) Intracortical facilitation and inhibition after transcranial magnetic stimulation in conscious humans. J Physiol 498 (Pt 3):817-823.

Netoff T, Banks M, Dorval A, Acker C, Haas J, Kopell N, White J. (2005) Synchronizationn I Hybrid Neuronal Networks of the Hippocampal Formation. J Neurophysiol. 93:1197-1208

Nitsche MA, Paulus W (2000) Excitability changes induced in the human motor cortex by weak transcranial direct current stimulation. J Physiol 527 Pt 3:633-639.

Nitsche MA, Liebetanz D, Antal A, Lang N, Tergau F, Paulus W (2003a) Modulation of cortical excitability by weak direct current stimulation--technical, safety and functional aspects. Suppl Clin Neurophysiol 56:255-276.

Nitsche MA, Fricke K, Henschke U, Schlitterlau A, Liebetanz D, Lang N, Henning S, Tergau F, Paulus W (2003b) Pharmacological modulation of cortical excitability shifts induced by transcranial direct current stimulation in humans. J Physiol 553:293-301.

Normann RA, Maynard EM, Rousche PJ, Warren DJ (1999) A neural interface for a cortical vision prosthesis. Vision Res 39:2577-2587.

Nowak LG, Bullier J (1998) Axons, but not cell bodies, are activated by electrical stimulation in cortical gray matter. I. Evidence from chronaxie measurements. Exp Brain Res 118:477-488.

Nunez PL, Srinivasan RS (2005) Electric Fields of the Brain: The Neurophysics of EEG. Oxford Univ. Press, Oxford

Parra LC, Bikson M (2004) Model of the effect of extracellular fields on spike time coherence. Conf Proc IEEE Eng Med Biol Soc 6:4584-4587.

Pascual-Leone A, Valls-Sole J, Wassermann EM, Hallett M (1994) Responses to rapid-rate transcranial magnetic stimulation of the human motor cortex. Brain 117 (Pt 4):847-858.

Patton HD, Amassian VE (1954) Single and multiple-unit analysis of cortical stage of pyramidal tract activation. J Neurophysiol 17:345-363.

Peterchev AV, Jalinous R, Lisanby SH (2008) A transcranial magnetic stimulator inducing near-rectangular pulses with controllable pulse width (cTMS). IEEE Trans Biomed Eng 55:257-266.

Plonsey R, Altman KW (1988) Electrical stimulation of excitable cells-a model approach. Proceedings of the IEEE 76:1122-1129.

Plonsey R, Barr RC (1998) Electric field stimulation of excitable tissue. IEEE Eng Med Biol Mag 17:130-137.

Purpura DP, McMurtry JG (1965) Intracellular Activities and Evoked Potential Changes During Polarization of Motor Cortex. J Neurophysiol 28:166-185.

Radman T, Ramos RL, Brumberg JC, Bikson M (2009 (in press)) Role of Cortical Cell Type and Morphology in Sub- and Suprathreshold Uniform Electric Field Stimulation Brain Stimulation.

Radman T, Su Y, An JH, Parra LC, Bikson M (2007) Spike timing amplifies the effect of electric fields on neurons: implications for endogenous field effects. J Neurosci 27:3030-3036.

Radman T, Parra LC, Bikson M. (2006) Amplification of small electric fields by neurons; implications for spike timing, 28th Annual International Conference of the IEEE Engineering in Medicine and Biology Society

Rall W (1977) Core conductor theory and cable properties of neurones. In: Handbook of Physiology: The Nervous System, section 1, vol. 1 (Brookhart JM, Mountcastle VB, eds), pp 39-97. Bethesda: American Physiology Society.

Ramos RL, Tam DM, Brumberg JC (2008a) Physiology and morphology of callosal projection neurons in mouse. Neuroscience 153:654-663.

Ramos RL, Smith PT, DeCola C, Tam D, Corzo O, Brumberg JC (2008b) Cytoarchitecture and transcriptional profiles of neocortical malformations in inbred mice. Cereb Cortex 18:2614-2628.

Ranck JB, Jr. (1975) Which elements are excited in electrical stimulation of mammalian central nervous system: a review. Brain Res 98:417-440.

Rattay F (1989) Analysis of models for extracellular fiber stimulation. IEEE Trans Biomed Eng 36:676-682.

Rattay F. (1998) Analysis of the electrical excitation of CNS neurons. IEEE Transactions on Biomedical Engineering 45(6):766-772

Riehle A, Grammont F, Diesmann M, Grun S. (2000) Dynamical changes and temporal precision of synchronized spiking activity in monkey motor cortex during movement preparation. J Physiol Paris. 94(5-6):569-82.

Reinagel P, Reid RC. (2000) Temporal coding of visual information in the thalamus. J Neurosci. 20(14):5392-400.

Rocco MM, Brumberg JC (2007) The sensorimotor slice. J Neurosci Methods 162:139-147.

Rotem A, Moses E (2008) Magnetic stimulation of one-dimensional neuronal cultures. Biophys J 94:5065-5078.

Roth BJ (1994) Mechanisms for electrical stimulation of excitable tissue. Crit Rev Biomed Eng 22:253-305.

Rothwell J, Burke D, Hicks R, Stephen J, Woodforth I, Crawford M (1994) Transcranial electrical stimulation of the motor cortex in man: further evidence for the site of activation. J Physiol 481 (Pt 1):243-250.

Rudiak D, Marg E (1994) Finding the depth of magnetic brain stimulation: a re-evaluation. Electroencephalogr Clin Neurophysiol 93:358-371.

Sayer, R., M. Friedlander, and S. Redman, The time course and amplitude of EPSPs evoked at synapses between pairs of CA3/CA1 neurons in the hippocampal slice. J. Neurosci., 1990. **10**(3): p. 826-836.

Sarnthein J., Jeanmonod D. (2007) High thalamocortical theta coherence in patients with Parkinson's disease. J. Neurosci. 27(1): 124-131

Schaefer AT, Angelo K, Hartwig S, Margrie T (2006) Neuronal oscillations enhance stimulus discrimination by ensuring action potential precision PLOS Biology 4(6): 1010-24

Scherberger H, Jarvis MR, Andersen RA (2005) Cortical local field potential encodes movement intentions in the posterior parietal cortex. Neuron 46: 347-354

Schneidman E, Freedman B, Segev I. (1998) Ion channel stochasticity may be critical in determining the reliability and precision of spike timing. Neural Computation 10:1679-1703

Shu Y, Hasenstaub A, Badoual M, Bal T, McCormick D.A. (2003) Barrages of Synaptic Activity Control the Gain and Sensitivity of Cortical Neurons. J. Neurosci. 23(32):10388-10401

Siapas AG, Lubenov EV Wilson MA. (2005) Prefrontal Phase Locking to Hippocampal Theta Oscillations. Neuron 46:114

Sommer M, Lang N, Tergau F, Paulus W (2002) Neuronal tissue polarization induced by repetitive transcranial magnetic stimulation? Neuroreport 13:809-811.

Svirskis G, Baginskas A, Hounsgaard J, Gutman A (1997) Electrotonic measurements by electric field-induced polarization in neurons: theory and experimental estimation. Biophys J 73:3004-3015.

Takano B, Drzezga A, Peller M, Sax I, Schwaiger M, Lee L, Siebner HR (2004) Short-term modulation of regional excitability and blood flow in human motor cortex following rapid-rate transcranial magnetic stimulation. Neuroimage 23:849-859.

Tehovnik EJ, Tolias AS, Sultan F, Slocum WM, Logothetis NK (2006) Direct and indirect activation of cortical neurons by electrical microstimulation. J Neurophysiol 96:512-521.

Terzuolo CA, Bullock TH (1956) Measurement of Imposed Voltage Gradient Adequate to Modulate Neuronal Firing. Proc Natl Acad Sci U S A 42:687-694.

Thielscher A, Kammer T (2002) Linking physics with physiology in TMS: a sphere field model to determine the cortical stimulation site in TMS. Neuroimage 17:1117-1130.

Tranchina D, Nicholson C (1986) A model for the polarization of neurons by extrinsically applied electric fields. Biophys J 50:1139-1156.

Trussell LO. (1999) Synaptic mechanisms for coding timing in auditory neurons. Annu Rev Physiol. 61:477-96.

Uy J, Ridding MC (2003) Increased cortical excitability induced by transcranial DC and peripheral nerve stimulation. J Neurosci Methods 127:193-197.

Valero-Cabre A, Payne BR, Rushmore J, Lomber SG, Pascual-Leone A (2005) Impact of repetitive transcranial magnetic stimulation of the parietal cortex on metabolic brain activity: a 14C-2DG tracing study in the cat. Exp Brain Res 163:1-12.

Wagner T, Valero-Cabre A, Pascual-Leone A (2007a) Noninvasive human brain stimulation. Annu Rev Biomed Eng 9:527-565.

Wagner T, Fregni F, Fecteau S, Grodzinsky A, Zahn M, Pascual-Leone A (2007b) Transcranial direct current stimulation: a computer-based human model study. Neuroimage 35:1113-1124.

Wassermann EM, Wang B, Zeffiro TA, Sadato N, Pascual-Leone A, Toro C, Hallett M (1996) Locating the motor cortex on the MRI with transcranial magnetic stimulation and PET. Neuroimage 3:1-9.

Webster BR, Celnik PA, Cohen LG (2006) Noninvasive brain stimulation in stroke rehabilitation. NeuroRx 3:474-481.

Yang CR, Seamans JK, Gorelova N (1996) Electrophysiological and morphological properties of layers V-VI principal pyramidal cells in rat prefrontal cortex in vitro. J Neurosci 16:1904-1921.